SMHI

Nr 81, 2005

Oceanografi

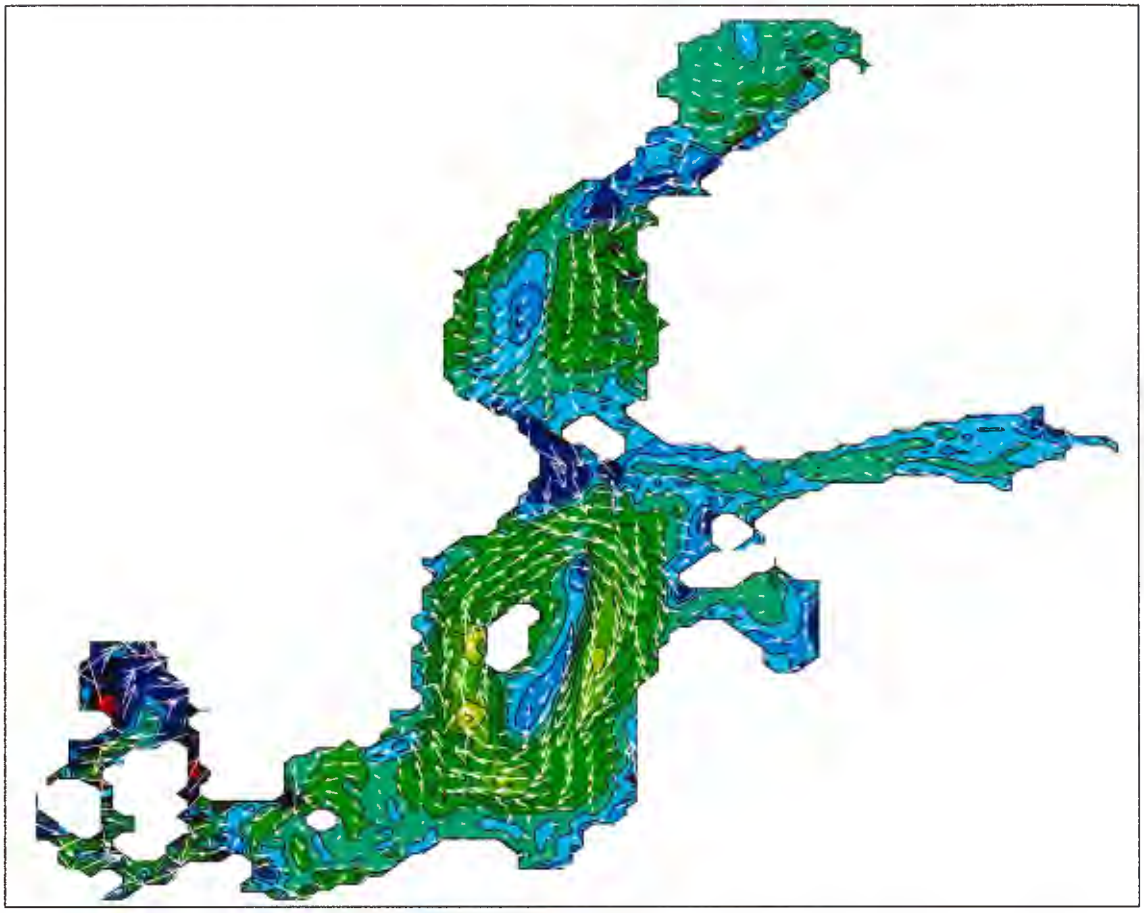

Implementation of a Flux Corrected Transport scheme in the Rossby Centre Ocean model

Tobias Strömgren
Master of Science Thesis, 2005
Supervisor Markus Meier, SMHI
Examinator Dan S. Henningson, KTH

Cover illustration: Average surface velocity field for the period 1903 – 1998. For details see figure 5.10.

Oceanografi
Nr 81, 2005

Implementation of a Flux Corrected Transport scheme in the Rossby Centre Ocean model

Tobias Strömgren
Master of Science Thesis, 2005
Supervisor Markus Meier, SMHI
Examinator Dan S. Henningson, KTH

Report Summary / Rapportsammanfattning

Issuing Agency/Utgivare	Report number/Publikation
Swedish Meteorological and Hydrological Institute S-601 76 NORRKÖPING Sweden	Oceanografi Nr 81
	Report date/Utgivningsdatum May 2005

Author (s)/Författare

Tobias Strömgren

Title (and Subtitle/Titel

Implementation of a flux Corrected Transport scheme in the Rossby Centre Ocean model

Abstract/Sammandrag

Two different advection schemes, Flux Corrected Transport (FCT) scheme (Zalesak, 1979) and incremental remapping (Dukowicz and Baumgardner, 2000) have been tested in a two-dimensional test program where an initial cylindrical tracer distribution was advected in a circular velocity field. Evaluation of the tests showed that incremental remapping preserved the shape of the tracer distribution better than FCT. However, incremental remapping is computationally efficient first when many tracers are used. In addition, it has been developed for only two-dimensions so far. Consequently, it was decided to implement FCT into the Rossby Centre Ocean model (RCO) (Meier et al., 1999).

Model simulations with RCO for the period November 1902 to December 1998 were done with FCT as advection scheme. This model simulation was compared to a model simulation with modified split-quick (Webb et al., 1997) advection scheme (Meier and Kauker, 2003). Modified split-quick is a third order scheme and is the current advection scheme in RCO.

The advection of salinity and temperature was compared between the two model simulations. FCT was applied without explicit diffusion whereas modified split-quick needs explicit diffusion to eliminate subgrid-scale noise caused by the non-monotonicity of the scheme. Consequently, the simulation utilizing FCT was less diffusive. This is positive because as little implicit diffusion as possible is desirable, especially for long integrations. At sharp gradients modified split-quick may result in under- or overshooting. For example at the outflow of Neva and Kemijoki rivers a sharp salinity gradient causes salinity to become negative for modified split-quick. FCT was shown to handle sharp gradients very well, no negative values for the salinity occurs with FCT as advection scheme.

Key words/sök-, nyckelord

Numerical modelling, advection scheme, Baltic Sea, climate variability

Supplementary notes/Tillägg	Number of pages/Antal sidor	Language/Språk
Master of Science Thesis Supervisor H. E. Markus Meier, SMHI Examinator Dan. S. Henningson, KTH	40	English

ISSN and title/ISSN och titel

0283-7714 SMHI Oceanografi

Report available from/Rapporten kan köpas från:

SMHI
S-601 76 NORRKÖPING
Sweden

Contents

Chapter 1

Introduction

Three-dimensional ocean circulation models are widely used to investigate ocean climate. They are built upon the primitive equations which are derived from the Navier-Stokes equations with the following approximations: The Boussinesq approximation where the ocean is regarded as incompressible, the spherical approximation approximating the earth with a sphere, the hydrostatic approximation stating that the pressure only has a static component and the traditional approximation that neglects the component of the Coriolis force due to vertical current velocity. For details see Müller and Willebrand (1989), Meier et al. (1999) and Döös (2004).

With these approximations the Navier-Stokes equation become,

$$\frac{\partial \mathbf{u}}{\partial t} + (\mathbf{u} \cdot \nabla_h)\mathbf{u} + w\frac{\partial \mathbf{u}}{\partial z} + \mathbf{f} \times \mathbf{u} = -\frac{a}{\rho_0}\nabla_h p + \mathbf{D_u} + \mathbf{F_u} \tag{1.1}$$

where $\mathbf{u} = (u, v)$ are the horizontal velocity, w the vertical velocity, $\mathbf{f}$ the Coriolis term, $\nabla_h = (\frac{\partial}{\partial x}, \frac{\partial}{\partial y})$, $\mathbf{D_u}$ the diffusion and $\mathbf{F_u}$ a forcing term.

The advection-diffusion equation for a tracer, T, is

$$\frac{\partial T}{\partial t} + ((\mathbf{u}, w) \cdot \nabla)T = D_T + F_T \tag{1.2}$$

where D is diffusion and F is a source term.

With equation 1.1 and 1.2 the horizontal velocity, the salinity and temperature can be calculated. From these the pressure, the vertical velocity and the density can be derived.

The Rossby Centre Ocean model (RCO) has been developed based on OCCAM (Ocean Circulation Climate Advanced Modelling Project in Southampton). Today RCO and OCCAM use the so-called modified split-quick scheme for advection (Webb et al., 1997). This advection scheme is computationally efficient but nevertheless suffer from the shortcoming of not preserving monotonicity. This is a problem where the gradient of salinity is large i.e. at river mouths. At these large gradients the salinity can become negative. This may also be a problem for additional tracers (other than temperature and salinity) during long integrations and for the coupling with a biogeochemical model, when an accurate advection of the tracers is necessary (H.E.M. Meier, pers.comm.).

The aim of this master thesis is to implement a new advection scheme into RCO. An ideal advection scheme would have the following features:

- The scheme should be conservative.
- The scheme should be stable.
- The scheme should be second order accurate.
- The scheme should preserve monotonicity of the conserved fields and tracers, i.e. no new maxima or minima should be created under non-divergent transport.
- The method should be computationally efficient.

In this master thesis two advection schemes are studied. The Flux Corrected Transport scheme (FCT) developed by Zalesak (1979) is presented in section 2.1. An advection scheme with incremental remapping by Dukowicz and Baumgardner (2000) is presented in section 2.2. FCT has earlier been evaluated by Gerdes et al. (1991) with satisfying results. Incremental remapping is a new method under development at Los Alamos Laboratories and it has been used in two dimensions for an sea-ice model (Lipscomb (2001); Hunke and Lipscomb (2004)). These two advection schemes are compared in section 3.2 in 2-dimensional test runs. The implementation of FCT in the Rossby Centre Ocean model (RCO) is described in section 4. Test runs are made with the FCT scheme in RCO and compared with the current advection scheme in RCO, the modified split-quick (Webb et al. (1997); Meier and Kauker (2003)) in section 5. Conclusions in section 6.

Chapter 2

Methods

2.1 FCT algorithm

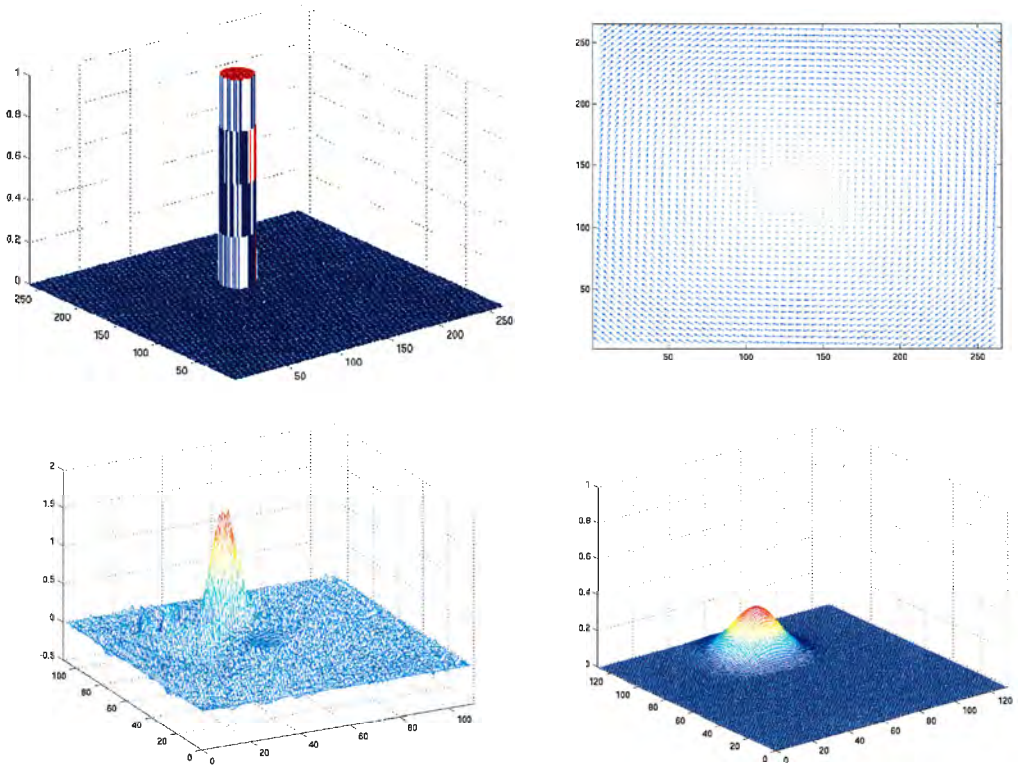

Figure 2.1: An initial cylindrical tracer distribution is advected one revolution in a cylindrical velocity field with the central difference scheme and the upstream scheme. Top left: Initial tracer distribution. Top right: Circular velocity field. Bottom left: Central difference after one revolution. Bottom right: Upstream after one revolution.

The FCT algorithm is a combination of a high order and a low order method. Numerical integration of the advection equation with a high order scheme is very dispersive,

particularly near steep gradients, see figure 2.1. A low order scheme is not dispersive and positivity preserving, but very diffusive, see figure 2.1. Here central difference is used as a high order scheme and upstream as a low order scheme. The upstream scheme is sign preserving but very diffusive, the central difference scheme is not that diffusive but very dispersive and not sign preserving, see figure 2.1.

FCT is a compromise between the upstream and the central difference scheme. It takes advantages of their respective benefits and limits their drawbacks. The flux difference (anti-diffusive flux) between the central difference and the upstream scheme is computed. The central idea is to limit the anti-diffusive flux locally such that no under- or overshoots are introduced. This corrected anti-diffusive flux is then added to the upstream (low order) solution. Before the anti-diffusive fluxes are corrected DeVore's prelimiter is added (Danielson and Haulin, 2004). This limits the anti-diffusive fluxes in each direction so that creation and enhancement of directional extrema is prevented and anti-diffusive fluxes directed down the gradient of the low order solution are reversed. To be stable the algorithm must fulfill the CFL restriction, $\frac{|\mathbf{u}|\Delta t}{\Delta x} < 1$. The FCT algorithm is developed by Zalesak (1979). For details see also Kunhardt and Wu (1987).

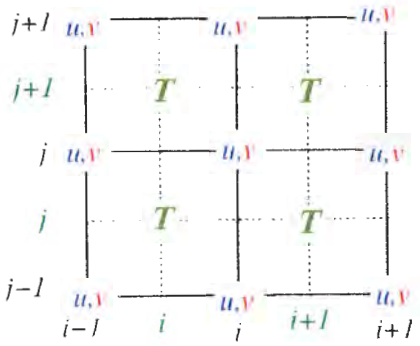

Figure 2.2: The relative locations of the velocities u,v and a tracer T on an Arakawa-B grid, adopted from Danielson and Haulin (2004).

2.1.1 Description of the code

The code describing the FCT algorithm is written in Fortran 90 by Danielson and Haulin (2004). Here the FCT algorithm is from Zalesak (1979) with DeVore's prelimiter. To make test runs I have made an own driver routine where an initial tracer field is set and a velocity field is created. The algorithm is changed from a latitude-longitude coordinate system to a Cartesian grid. Velocity and tracer fields are defined on an Arakawa B-grid, tracers are defined in the center of a cell and velocities at the corners (Fig. 2.2). In the tracer subroutine the tracer is updated with the FCT scheme for each time step. Below I will show the steps in the x-direction of the three dimensional algorithm in the tracer subroutine.

1. The upstream flux, $F^U_{k,i+(1/2),j}$, is calculated for the x-direction of each cell.

2. The solution for upstream, $T^U_{k,i,j}$, is calculated at all points for the next time step.

$$T^U_{k,i,j} = T^n_{k,i,j} - \frac{1}{V_{k,i,j}}(F^U_{k,i+(1/2),j} - F^U_{k,i-(1/2),j} + F^U_{k,i,j+(1/2)} - F^U_{k,i,j-(1/2)} + F^U_{k+(1/2),i,j} - F^U_{k-(1/2),i,j}) \tag{2.1}$$

Where $V_{k,i,j}$ is the volume and $T^n_{k,i,j}$ is the FCT solution of the current time step.

3. The central difference flux, $F^{CD}_{k,i+(1/2),j}$, is calculated for the x-direction of each cell.

4. Anti-diffusive fluxes for all points are calculated by taking the difference between central difference and upstream fluxes.

$$A_{k,i+(1/2),j} \equiv F^{CD}_{k,i+(1/2),j} - F^U_{k,i+(1/2),j} \tag{2.2}$$

5. DeVore's prelimiter is calculated for each direction.

$$A'_{k,i+(1/2),j} = S_{k,i+(1/2),j} max\{0, min(\mid A_{k,i+(1/2),j} \mid , S_{k.i+(1/2),j} V_{k,i,j} \Delta T^U_{k,i-(1/2),j} , S_{k,i+(1/2),j} V_{k,i,j} \Delta T^U_{k,i+(3/2),j})\} \tag{2.3}$$

$$\Delta T^U_{k,i+(1/2),j} \equiv T^U_{k,i+1,j} - T^U_{k,i,j} \tag{2.4}$$

$$S_{k,i+(1/2),j} \equiv sign(\Delta T^U_{k,i+(1/2),j}) \tag{2.5}$$

6. The anti-diffusive fluxes are multiplied with Zalesaks limiter.

$$A^C_{k,i+(1/2),j} = C_{k,i+(1/2),j} A'_{k,i+(1/2),j} \tag{2.6}$$

where

$$C_{k,i+(1/2),j} = min(R^+_{k,i+1,j}, R^-_{k,i,j}) \quad if A'_{k,i+(1/2),j} \geq 0 \tag{2.7}$$

$$C_{k,i+(1/2),j} = min(R^+_{k,i,j}, R^-_{k,i+1,j}) \quad if A'_{k,i+(1/2),j} < 0 \tag{2.8}$$

where

$$R^{\pm}_{k,i,j} = min(1, Q^{\pm}_{k,i,j}/(P^{\pm} + \varepsilon)) \tag{2.9}$$

$$Q^+_{k,i,j} = T^{max}_{k,i,j} - T^U_{k,i,j} \tag{2.10}$$

$$Q^-_{k,i,j} = T^U_{k,i,j} - T^{min}_{k,i,j} \tag{2.11}$$

$P^+_{k,i,j}$ and $P^-_{k,i,j}$ are the sums of all anti-diffusive fluxes into and out from a grid box (k,i,j), respectively.

$$T^{a/b}_{k,i,j} = max/min(T^n_{k,i,j}, T^U_{k,i,j}) \tag{2.12}$$

$$T^{max/min}_{k,i,j} = max/min(T^{a/b}_{k-1,i,j}, T^{a/b}_{k+1,i,j}, T^{a/b}_{k,i-1,j}, T^{a/b}_{k,i+1,j}, T^{a/b}_{k,i,j-1}, T^{a/b}_{k,i,j+1}, T^{a/b}_{k,i,j}) \tag{2.13}$$

7. The tracer is updated for all points and the program exits the tracer subroutine.

$$T^{n+1}_{k,i,j} = T^{U}_{k,i,j} - \frac{1}{V_{k,i,j}}(A^{C}_{k,i+(1/2),j} - A^{C}_{k,i-(1/2),j} + A^{C}_{k,i,j+(1/2)}$$

$$-A^{C}_{k,i,j-(1/2)} + A^{C}_{k+(1/2),i,j} - A^{C}_{k-(1/2),i,j}) \tag{2.14}$$

Over each of the parts 1 to 7 of the scheme there are loops over x, y and z. The tracer field is written to ASCII-files by the driver routine for visualization with Matlab.

2.2 Incremental remapping

Incremental remapping is different from the most common way to numerically solve the advection equation, to discretize the equation in space, and to step it forward in time. Cell volumes are projected backward or forward along Lagrangian trajectories, the resulting tracer distribution is then remapped onto a target mesh.

The remapping method uses the fact that the advection equation 1.2 can be written in integral (conservative) form

$$\frac{D}{Dt}\int \phi dV = 0. \tag{2.15}$$

where

$$\frac{D}{Dt} = \frac{\partial}{\partial t} + \mathbf{u}\cdot\nabla \tag{2.16}$$

This equation fulfills the demand that the tracer, ϕ, should be conserved. The sum of a tracer is conserved along a trajectory. The total sum of a tracer is

$$T(t) = \int_{V_L} \phi dV \tag{2.17}$$

where V_L is a Lagrangian volume. A discretization of this is

$$T^{n+1} = T^{n}. \tag{2.18}$$

The Lagrangian cell-average density is defined as

$$\bar{\phi}(t) = \int_{V_L(t)} \phi dV \Big/ \int_{V_L(t)} dV = \frac{T(t)}{V_L(t)}. \tag{2.19}$$

This gives together with equation 2.18

$$\bar{\phi}^{n+1} = T(t^{n+1})/V_L(t^{n+1}) = T(t^{n})/V_L(t^{n+1}) = \bar{\phi}^{n} V_L(t^{n})/V_L(t^{n+1}). \tag{2.20}$$

Backward remapping is used here, this means that the target grid which is the desired grid at time t^{n+1} is projected back in time with the known velocities from the current time step. This gives us $V_L(t^n)$. The mean tracer value known for time step t^n are reconstructed to get ϕ^n_T using a linear approximation. A linear reconstruction makes the algorithm second order accurate. The gradients of the tracer are limited within the cell to preserve positivity

and monotonicity. The total tracer and the mean value of the tracer at the target grid are now

$$T_T^{n+1} = \int_{V_T} \phi_L^{n+1} dV \tag{2.21}$$

$$\bar{\phi}_T^{n+1} = T_T^{n+1}/V_T \tag{2.22}$$

The target grid is usually a regular grid to make the reconstruction easier.

The time step is not limited by a stability criterion but is restricted such that trajectories in neighboring grid cells do not cross, $max|\nabla \mathbf{u}|\Delta t < 1$. A remapping method with this restriction is called incremental remapping. Incremental remapping is by construction conservative.

Incremental remapping is a generally expensive scheme but most of the computational work is geometrical and is computed only once per time step. This information can be reused for tracers at the same time step which makes the method more efficient when many tracers are calculated. For details see Hunke and Lipscomb (2004), Dukowicz and Baumgardner (2000), Lipscomb (2001) and Dukowicz and Padial (1991).

2.2.1 Description of the code

Here follows a brief description of the code and how the algorithm is implemented. The code is taken from the Los Alamos Sea Ice Model (CICE, 2003). Some changes had to be done because the code is written for a sea-ice model. The code is modular and written in fixed-format FORTRAN 90. Only the tracer routine with necessary subroutines is used. To adapt it to the driver routine used for FCT changes were made to the incremental remapping code. The most important subroutines and changes in the code will be mentioned here so that the reader will be able to follow the scheme. For a more comprehensive description of the code see Hunke and Lipscomb (2004).

The module for horizontal transport with incremental remapping was adapted to the same driver routine that was used for FCT. First the grid is initialized. An Arakawa B-grid is used (Fig. 2.2). For simplicity the coordinate system is changed from latitude-longitudinal to a rectangular Cartesian coordinate system.

The steps in the tracer module are:

- The departure points of trajectories are calculated with a midpoint approximation, given the velocity field on the cell corners (Fig. 2.3).
- Knowing the departure points areas and vertices of flux triangles for east and north cell edges are computed. There are at most 5 triangles that can contribute to flux integrals for each edge. See figure 3 and table 1 in Dukowicz and Baumgardner (2000).
- The coordinates of the triangle points needed for the flux integrals are computed. The calculations so far are geometrical and are reused for all tracers.
- Tracer fields are computed at the geometric center of each cell. For second order accuracy a linear approximation is used. Monotonicity is ensured by a limiter.
- Fluxes are calculated across each edge by integrating the tracers over each flux triangle.

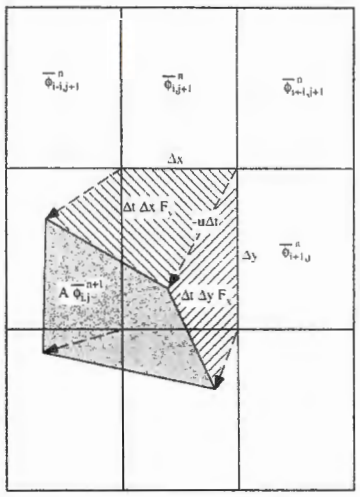

Figure 2.3: Backward-trajectory remapping of a two-dimensional cell, showing the shaded departure cell, the rectangular arrival cell, and the fluxing areas (marked with lines) associated with cell faces. Adopted from Dukowicz and Baumgardner (2000).

- The tracer is updated by summing the fluxes over each grid cell.

Chapter 3

Comparison between FCT and incremental remapping

3.1 Test runs

In order to decide which scheme should be implemented in the RCO model two different two-dimensional test cases, test case I and test case II (Tab. 3.1) have been carried out. In both problems a tracer is advected in a velocity field on a square domain subdivided into a uniform rectangular Arakawa-B grid of 265 x 265 cells (Fig.2.2). The velocity field corresponds to a uniform circular field around the center of the domain, $u = y_c \cdot c$, $v = -x_c \cdot c$, where x_c and y_c have their origin in the center of the domain and the constant c is the magnitude (Fig.2.1). The initial tracer distribution is given by a cylindrical distribution with one unit in amplitude and 14 units in radius. The cylinder is centered in $x = 133$, $y = 170$, 37 units above the center of the domain (Fig.2.1).

	Test case I	Test case II
Δt (s)	0.6	0.4
$\mathbf{u}_{max}$ (m/s)	0.5	2.2
$\mathbf{u}_c$ (m/s)	0.1	0.44
CFL	0.31	0.88
Δx, Δy (m)	1	1
One revolution (steps)	3770	1335

Table 3.1: Values for test case I and II. Δt is the time step. u_{max} is the maximum velocity. u_c is the velocity in the center of the initial tracer distribution. CFL = $\frac{|\mathbf{u}|\Delta t}{\Delta x}$ and Δx, Δy are the horizontal grid distance.

In general the mean circulation in the ocean amounts to about 0.1 m/s. The maximum speed in the Gulf stream is larger than 2 m/s. The CFL number for test case II is quite large. The largest CFL number allowed in RCO is 0.5.

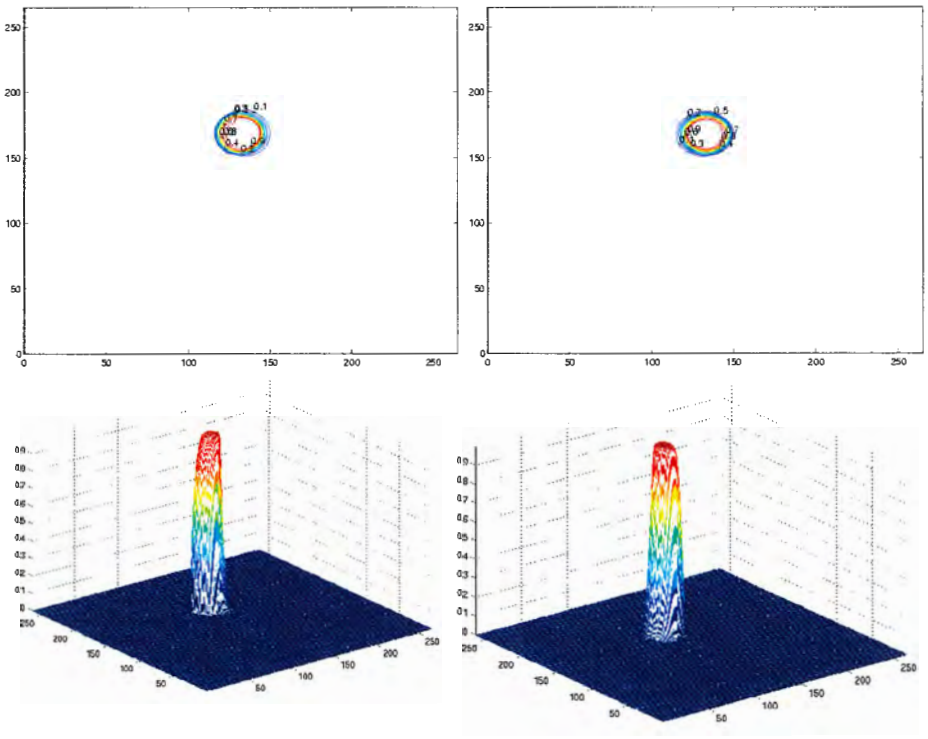

Figure 3.1: Test case I (see section 3.1) for one revolution of an initially cylindrical tracer distribution. Upper panels are contour plots and lower panels show tracer distributions. T_{max} is the maximum tracer value. Left: FCT, $T_{max} = 0.9999$. Right: Incremental remapping, $T_{max} = 0.9999$.

3.2 Results of the test runs

In test case I the results of the two schemes are quite similar after one revolution. Both schemes have very little diffusion. However the shape is better preserved by incremental remapping. Both schemes have a maximum tracer value of 0.999 (Fig.3.1).

After 10 revolutions the schemes differ more from each other. FCT doesn't preserve the shape of the tracer as well as incremental remapping. The tracer area is little larger for FCT (Fig.3.2).

After 20 revolutions the shape is better preserved for incremental remapping. Compared to other methods like central difference or upstream both incremental remapping and FCT have improved the results significantly (Fig.2.1). The maximum value of the tracers are almost the same: 0.915 for FCT and 0.921 for incremental remapping (Fig.3.3).

In test case II the speed is increased and the time step reduced. After one revolution the tracer distributions are similar to the one for test case I (Fig.3.4).

After 10 revolutions the tracer distribution is tall and narrow for FCT but still well preserved for incremental remapping. It is obvious that the higher speed affects the shape in case of FCT (Fig.3.5). The area greater than 0.9 is larger for FCT than for incremental remapping.

After 20 revolutions the distribution is so dispersed for FCT that it reaches the model

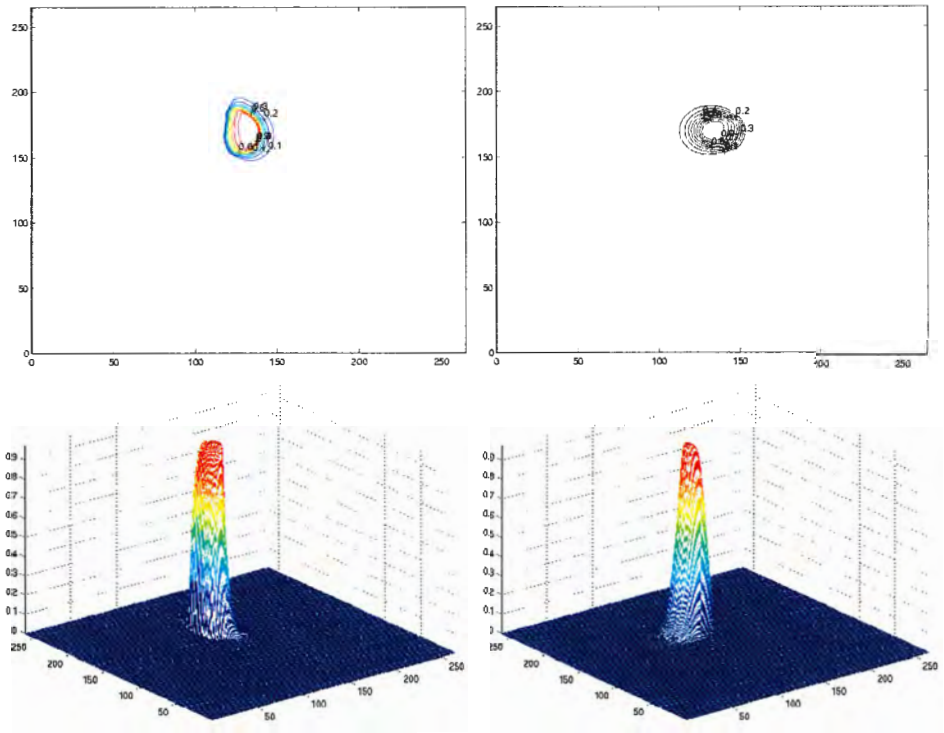

Figure 3.2: Test case I (see section 3.1) for 10 revolutions of an initially cylindrical tracer distribution. Upper panels are contour plots and lower panels show tracer distributions. T_{max} is the maximum tracer value. Left: FCT, $T_{max} = 0.9759$. Right: Incremental remapping, $T_{max} = 0.9770$.

boundary (Fig.3.6). The maximum tracer value is somewhat higher for FCT than incremental remapping. The maximum value of the tracer is slightly higher after 20 revolutions than for case I (Fig.3.7). The reason is that the same distance is calculated with less time steps.

A comparison of the computational costs between the two schemes after 2000 time steps shows: the FCT scheme needs 360 seconds for each tracer; within the incremental remapping scheme the geometrical part which is common for all tracers consumes 750 seconds; and each additional tracer needs 350 seconds. This means that incremental remapping is more computational efficient if there are more than 75 tracers. For one tracer FCT is three times faster than incremental remapping.

Although the FCT scheme is conservative the tracer start loosing concentration after 10 revolutions because no boundary conditions have been implemented (Fig.3.8). Reaching the border the tracer just vanishes (Fig.3.6).

3.3 Summary and discussion of the test run results

Both FCT and incremental remapping improve the results compared to central differences and upstream. None of the two schemes are dissipative like central differences or diffusive like upstream. Compared to each other, incremental remapping preserves the shape better

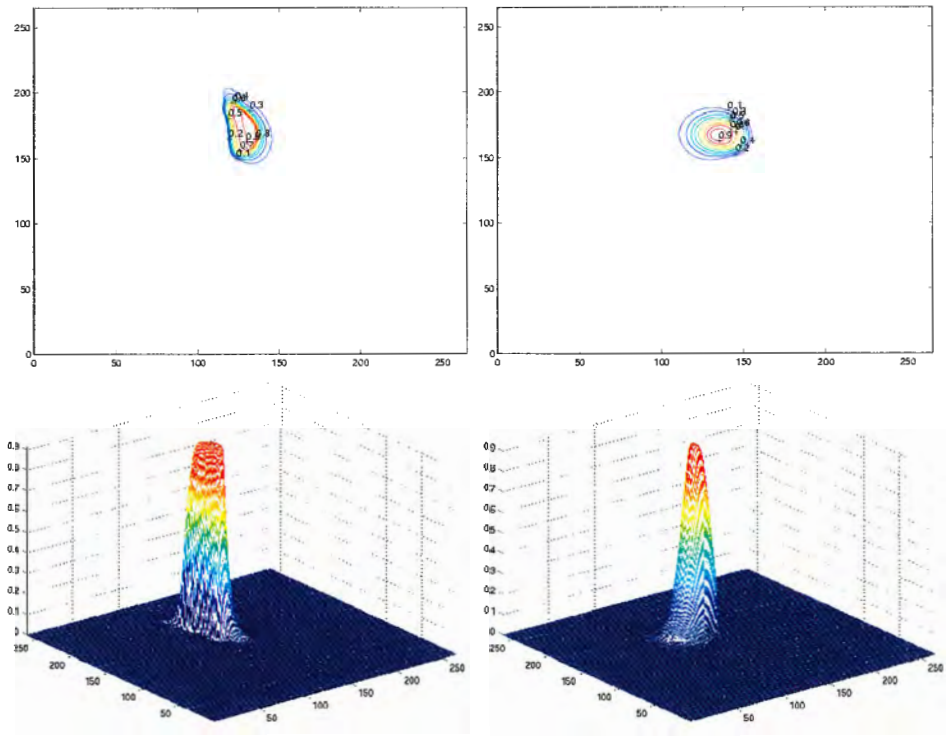

Figure 3.3: Test case I (see section 3.1) for 20 revolutions of an initially cylindrical tracer distribution. Upper panels are contour plots and lower panels show tracer distributions. T_{max} is the maximum tracer value. Left: FCT, $T_{max} = 0.9152$. Right: Incremental remapping, $T_{max} = 0.9209$.

than FCT, especially for high velocities. FCT preserves the amplitude a little better for high velocities and the area above 0.9 is larger for FCT. Incremental remapping is a more complicated algorithm compared to FCT.

Comparing test cases I and II it is visible that FCT is more diffusive for test case II where the velocity is more than four times higher. FCT seems to have a growing diffusion with velocity. The velocities in test case II are very high and it has a high CFL number. In the Baltic Sea the velocities are much lower in most parts. For incremental remapping the difference between the two test cases are negligible.

The main disadvantage for incremental remapping is that it is not developed for three dimensions. There is ongoing research to generalize incremental remapping to three dimensions. The other disadvantage is that it is computationally more expensive when the number of tracers is smaller than 75. In RCO around 10 tracers are calculated.

The main advantage of FCT is that it is cheaper than incremental remapping, already developed for three dimensions and easier to implement in RCO. Although the current time step must be changed for upstream, and the structure must be changed to fit into the same environment as the current advection scheme in RCO.

FCT seem to be the realistical algorithm to implement in RCO. FCT fulfills the requirements mentioned in section 1.

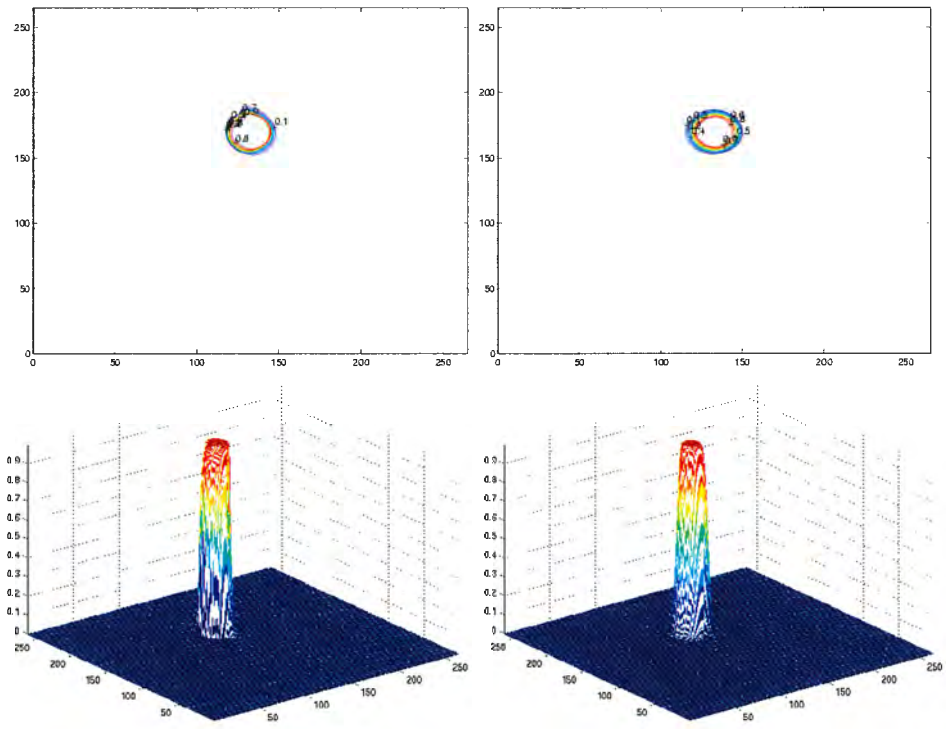

Figure 3.4: Test case II (see section 3.1) for one revolution of an initially cylindrical tracer distribution. Upper panels are contour plots and lower panels show tracer distributions. T_{max} is the maximum tracer value. Left: FCT, $T_{max} = 0.9999$. Right: Incremental remapping, $T_{max} = 0.9998$.

3.4 Diffusion coefficient for upstream.

To estimate the expected diffusion and to get a measure of how much of the tracer concentration disappears over the model boundary, the theoretical diffusion coefficient for upstream is calculated.

It is known that the first order upstream scheme corresponds to the second order central difference scheme with a diffusion coefficient on the right hand side. The details are shown below.

$$\frac{\partial T}{\partial t} + c\frac{\partial T}{\partial x} = \frac{\partial}{\partial x}(A\frac{\partial T}{\partial x}) \tag{3.1}$$

$$A = \frac{1}{2}c\Delta x \tag{3.2}$$

3.1 is discretized and developed

$$\frac{T_i^{n+1} - T_i^n}{\Delta t} + c\frac{T_{i+1}^n - T_{i-1}^n}{2\Delta x} = A\frac{T_{i+1}^n - 2T_i^n + T_{i-1}^n}{\Delta x^2} \tag{3.3}$$

$$\Rightarrow \frac{T_i^{n+1} - T_i^n}{\Delta t} + c\frac{T_{i+1}^n - T_{i-1}^n}{2\Delta x} = \frac{1}{2}c\Delta x\frac{T_{i+1}^n - 2T_i^n + T_{i-1}^n}{\Delta x^2} \tag{3.4}$$

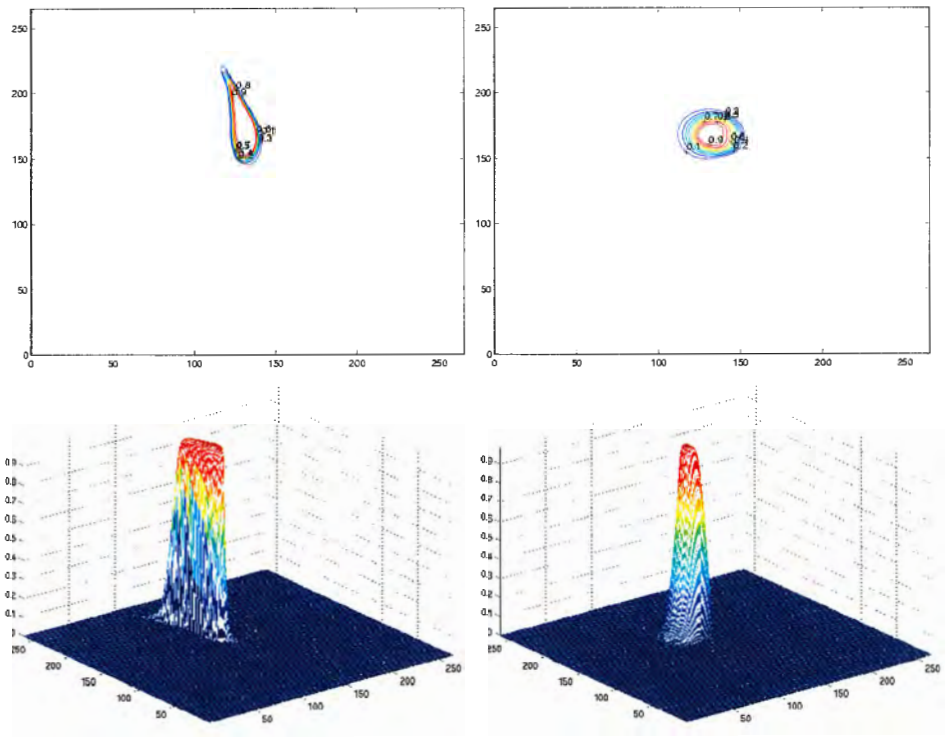

Figure 3.5: Test case II (see section 3.1) for 10 revolutions of an initially cylindrical tracer distribution. Upper panels are contour plots and lower panels show tracer distributions. T_{max} is the maximum tracer value. Left: FCT, $T_{max} = 0.9992$. Right: Incremental remapping, $T_{max} = 0.9892$.

$$\Rightarrow \frac{T_i^{n+1} - T_i^n}{\Delta t} + c\frac{T_{i+1}^n - T_{i-1}^n}{2\Delta x} = \frac{1}{2}c\frac{T_{i+1}^n - 2T_i^n + T_{i-1}^n}{\Delta x} \tag{3.5}$$

$$\Rightarrow \frac{T_i^{n+1} - T_i^n}{\Delta t} = \frac{1}{2}c\left(\frac{T_{i+1}^n - 2T_i^n + T_{i-1}^n - T_{i+1}^n + T_{i-1}^n}{\Delta x}\right) \tag{3.6}$$

$$\Rightarrow \frac{T_i^{n+1} - T_i^n}{\Delta t} = \frac{c}{2\Delta x}(2T_i^n - 2T_{i-1}^n) \tag{3.7}$$

$$\Rightarrow \frac{T_i^{n+1} - T_i^n}{\Delta t} + \frac{T_i^n - T_{i-1}^n}{\Delta x} = 0 \tag{3.8}$$

Thus central differences and diffusion corresponds to the upstream scheme. To estimate the time scale of diffusion the following equation is considered

$$\frac{\partial T}{\partial t} = \frac{\partial}{\partial x}A\frac{\partial T}{\partial x}. \tag{3.9}$$

Scaling results in

$$\frac{T}{t_0} = \frac{AT}{L^2} \tag{3.10}$$

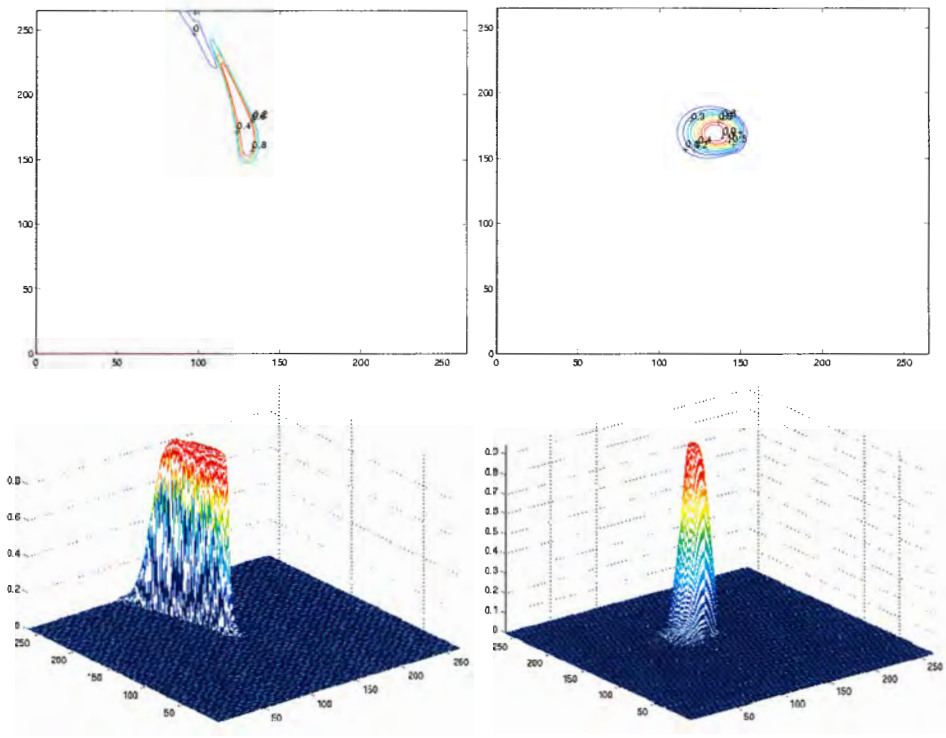

Figure 3.6: Test case II (see section 3.1) for 20 revolutions of an initially cylindrical tracer distribution. Upper panel are contour plots and lower panels show tracer distributions. T_{max} is the maximum tracer value. Left: FCT, $T_{max} = 0.9705$. Right: Incremental remapping, $T_{max} = 0.9501$.

$$\Rightarrow t_0 = \frac{2L^2}{c\Delta x} \tag{3.11}$$

where

t_0 = time scale for diffusion.

L = length scale $\sim$ the radius of the tracer distribution.

c = velocity scale $\sim$ the velocity in the center of the tracer distribution.

Δx = grid distance.

A theoretical estimation is that the maximum amplitude changes according to $e^{-\frac{t}{t_0}}$. To check the utilized discretizations the maximum amplitude of upstream with different t_0 was compared to the theoretical estimation $e^{-\frac{t}{t_0}}$. In Figure 3.9 the maximum amplitude of the tracer is plotted with the theoretical estimation for $t_0 = 811$ and $t_0 = 1622$. As one can see the theory corresponds quite well with the numerical upstream solution. To minimize the diffusion one should choose either small Δx or a small velocity. Note that diffusion is growing with velocity.

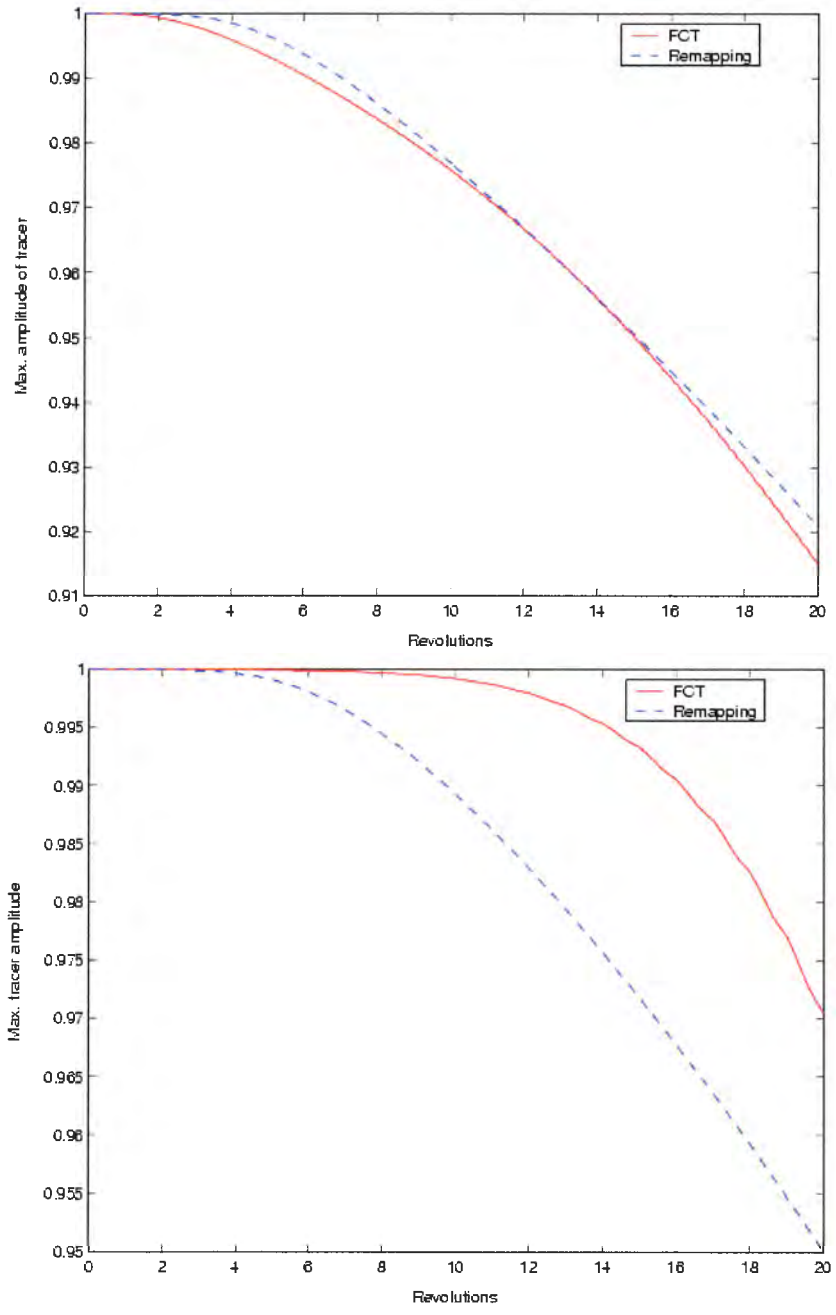

Figure 3.7: Top: Maximum amplitude of the tracer for test case I (see section 3.1). Bottom: Maximum amplitude of the tracer for test case II (see section 3.1).

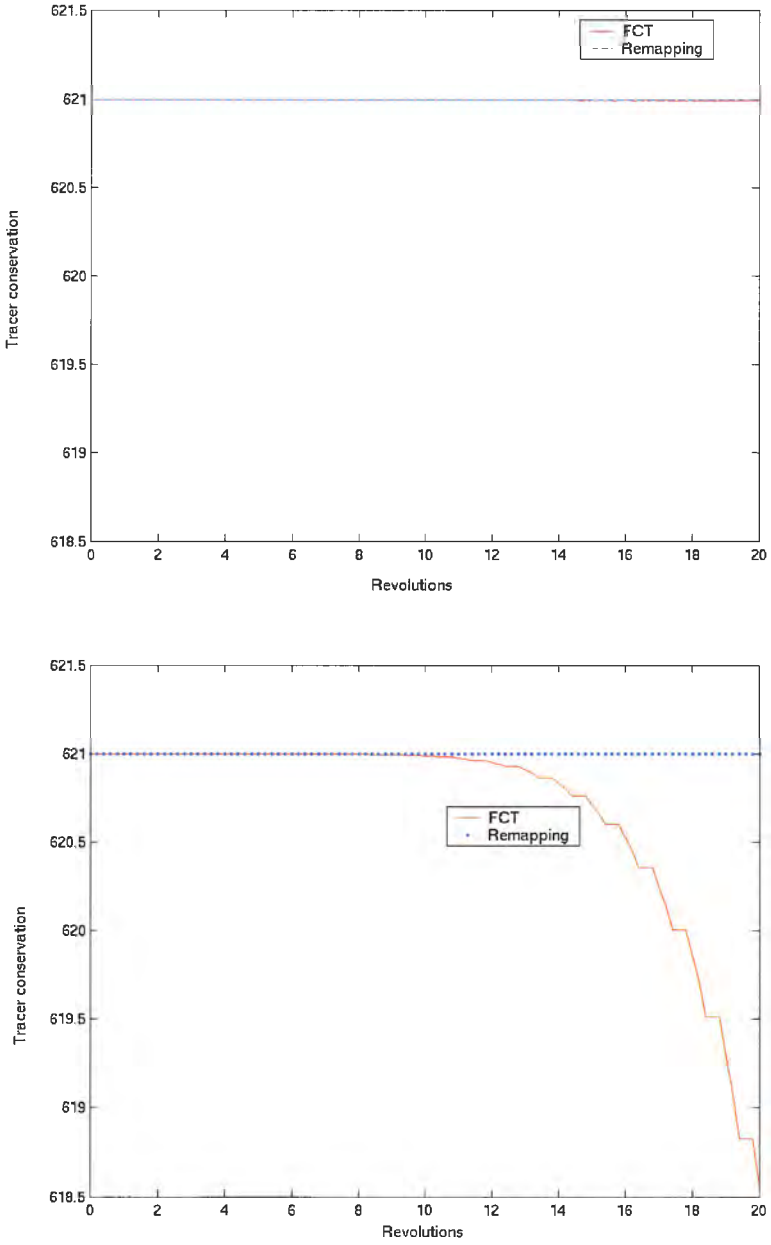

Figure 3.8: Top: Conservation of the tracer density for test case I (see section 3.1). Bottom: Conservation of tracer density for test case II (see section 3.1.

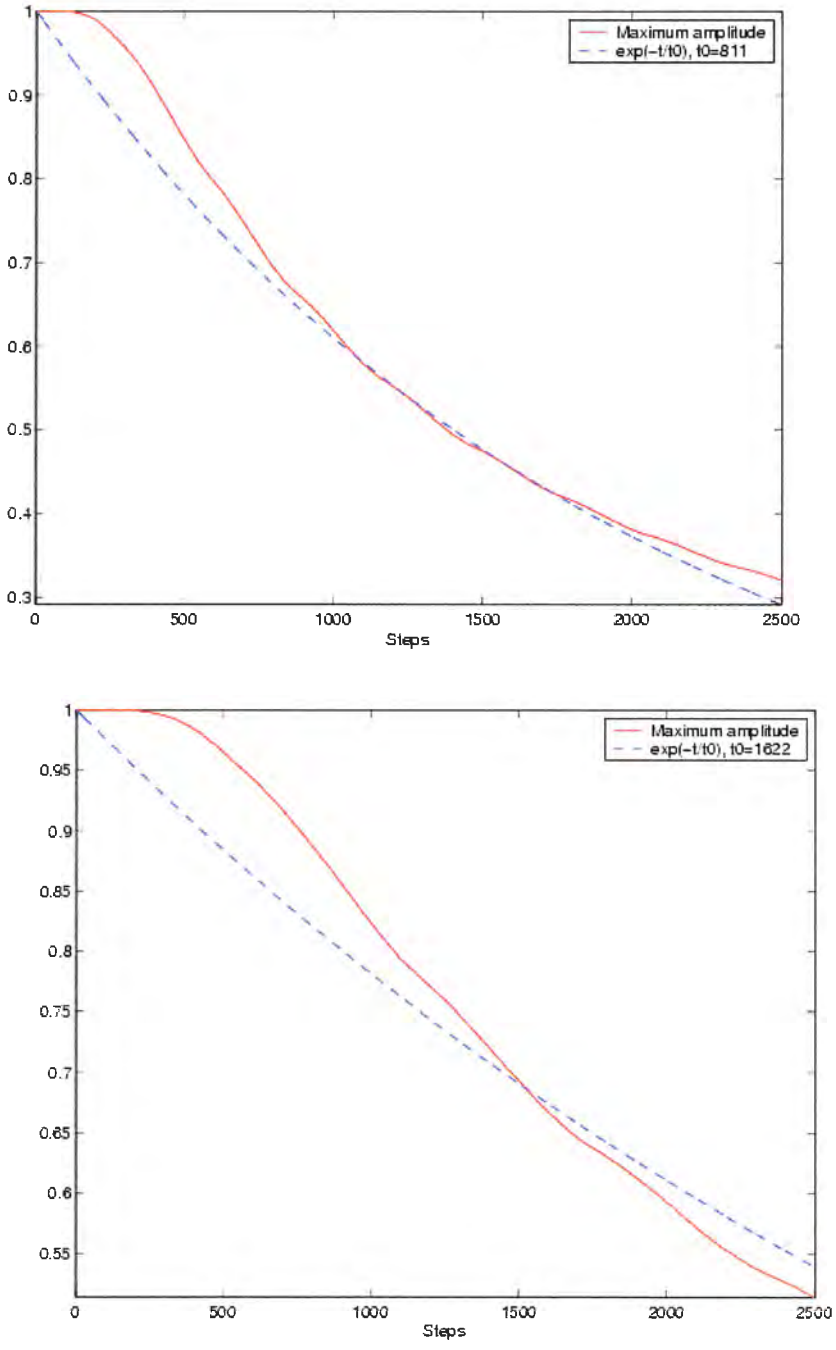

Figure 3.9: Maximum amplitude of the tracer with the theoretical estimation for different time scale diffusion, t_0. Top: $t_0 = 811$. Bottom: $t_0 = 1622$.

Chapter 4

Implementation in RCO

The Rossby Centre Ocean model, RCO, was developed by the Rossby Center at SMHI using OCCAM (Ocean Circulation Climate Advanced Modelling project in Southampton), which is built on the primitive equations derived from the Navier-Stokes equations using the same assumptions as in section 1. RCO was developed to study climate variability and change of the Baltic Sea and Arctic Ocean (Meier et al., 1999). The model is driven with daily sea level observations in Kattegat, monthly basin-wide discharge data and atmospheric data (Meier and Kauker, 2003). It is a fully three-dimensional model, written in Fortran77. It is parallelized with MPI and uses the Master-Slave arrangement with one master processor dedicated to external I/O and house-keeping tasks. Each slave processor receives the data it needs to perform the calculations in the domain assigned to it. The time loop is in the slave processors and for each time step the tracer routine is called once for each horizontal point. The model is run at the National Supercomputer Centre in Linköping, Sweden. There are many subroutines in RCO, but here only two subroutines will be studied. The tracer subroutine, *tracer.F*, where the tracer is advected and *step.F* where the horizontal loops are and where the tracer subroutine is called. Only the advection of tracers is changed, not the advection of velocities. For more information about RCO see Meier et al. (1999).

To implement the FCT-algorithm into RCO some changes have to be made in the program to fit into the RCO structure. The first problem to be solved is the time step. In RCO a leapfrog time step is used and in every 96:th time step an Euler forward time step is used to suppress the numerical mode. In the test program, see section 2.1, an Euler forward time step is used in upstream.

$$\mathbf{T^{n+1}} = \mathbf{T^n} - \Delta t \nabla \cdot (\mathbf{u^n T^n}) \tag{4.1}$$

One way to solve the problem would be to simply use an Euler forward time step in RCO, but this scheme would not be stable. Instead the time step discretization in the upstream scheme is changed to

$$\mathbf{T^{n+1}} = \mathbf{T^{n-1}} - 2\Delta t \nabla \cdot (\mathbf{u^n T^{n-1}}) \tag{4.2}$$

$\mathbf{u^n}$ has to be used because otherwise the scheme is unstable (Gerdes, 1988).

In RCO the tracer subroutine is called once for each horizontal point, (x,y), not once for each time step as in our test program in section 2.1.1. Inside the tracer subroutine there are only loops in the vertical direction, because they are optimized for the parallelization

in the horizontal. But in the test program in section 2.1.1 the neighboring points of the Zalesak's limiter are needed to update the tracer in one point. To calculate the neighboring points of Zalesak's limiter the neighboring points of DeVore's prelimiter are needed and so on all the way to the low-order flux.

There are two different ways to implement FCT, one is to use the same structure as in 2.1.1. In that case the steps 1 to 6 in section 2.1.1 are implemented outside the horizontal loops in *step.F*. Around this there is a loop over the number of tracers. The fields must then be a function of tracer, x, y and z, i.e. 4-dimensional. The tracer fields are updated in *tracer.F*. The two outermost points of the processor must be sent with message passing to its neighbor processors. Totally three 4-dimensional and four 3-dimensional fields must be sent and received with message passing which is quite time consuming. If message passing not is used one can loop over $i_{max}+2$, $j_{max}+2$, where i_{max}, j_{max} are the maximum x and y values in the current processor. The grid is unstructured. Thus points outside the grid will also be calculated, which causes some extra calculation.

The other way is to implement the FCT algorithm in *tracer.F* with the current loops in RCO. For each horizontal point there is a loop over k. No message passing is used here, so one dimensional fields can be used. For every horizontal point one also needs the vertical velocity, fluxes and T^U for the surrounding points. For every point, 22 extra fluxes need to be calculated and these can not be saved for other points. They will therefore be calculated several times. This is very inefficient.

In the model simulations, section 5, the same structure of FCT, as in section 2.1.1, is kept and implemented in *step.F*.

A slightly different way to calculate the allowed extremes of the tracer, $T_{max/min}$, is used here. Instead of calculating $T_{max/min}$ as in equation 2.13 we calculate it as

$$\begin{aligned} T_{k,i,j}^{max/min} = \{&T_{k,i,j}^U, T_{k,i,j}^n, \frac{1}{2}(T_{k,i,j}^n + T_{k,i+1,j}^n), \frac{1}{2}(T_{k,i,j}^n + T_{k,i-1,j}^n), \\ &\frac{1}{2}(T_{k,i,j}^n + T_{k,i,j+1}^n), \frac{1}{2}(T_{k,i,j}^n + T_{k,i,j-1}^n), \\ &\frac{1}{2}(T_{k,i,j}^n + T_{k+1,i,j}^n), \frac{1}{2}(T_{k,i,j}^n + T_{.k+1i,j}^n)\}. \end{aligned} \tag{4.3}$$

As one can see the upstream solutions $T_{k,i+1,j}^U$ are replaced by the mean of neighboring T^n. This is because with the implementation in section 2.1.1 points that lie outside the overlap are needed. This change gives very small influence to the solution. If a neighbor point is a land point it should be replaced with a sea point, for example $\frac{1}{2}(T_{k,i,j}^n + T_{k,i+1,j}^n)$ should be replaced with $T_{k,i,j}^n$ if $T_{k,i+1,j}^n$ is a land point (Gerdes, 1988).

DeVore's prelimiter is not used in the implementation in RCO because it needs information from (ic $\pm$ 3, jc $\pm$ 3), where ic is the central point. In RCO information from the two outermost points are sent to the neighboring processors.

Chapter 5

Model simulation with RCO

For validation of the new advection scheme a model simulation was made. The results are compared to the results of a model simulation using the current advection scheme, the modified split-quick scheme. The model simulation is made with 6nm (nautical miles) resolution in horizontal and 41 levels in the vertical direction for the period November 1902 to December 1998 (Meier and Kauker, 2003). The grid points in the vertical direction are unevenly distributed with increasing intervals between 3 m close to the surface and 12 m near the bottom. The time step is 600 seconds. Explicit diffusion is added to the modified split-quick scheme so that it stays stable. No explicit diffusion is added to FCT. Henceforth I will refer to the model simulation with the modified split-quick scheme as REF and to the model simulation with FCT as advection scheme as FCT. All difference plots are REF minus FCT.

With a 6nm horizontal resolution it is impossible to state if the new advection scheme gives a better approximation of the motions in the ocean. In order to do that a finer grid has to be used and results have to be compared with field observations. But with a 6nm model simulation it is possible to roughly state how the new advection scheme seems to work and see tendencies compared to REF.

In this configuration REF is about 2.2 times faster than FCT. Theoretically REF should be 2 times faster. It is expected that FCT will be slower because some extra grid points for each processor are calculated, see section 4.

5.1 Salinity and temperature at Arkona Deep, Bornholm Deep, and Gotland Deep

Figures 5.1 to 5.3 show salinity and temperature as a function of time and depth at Arkona Deep, Bornholm Deep and Gotland Deep. The plots over Arkona and Bornholm are filtered with a 4-year running mean.

At Arkona Deep (55.0 °N, 14.1 °E) the salinity close to the bottom is about 0.4 psu (practical salinity units) higher for FCT than for REF (Fig.5.1). About 5 m higher up REF gives about 0.7 psu higher salinity than FCT. Closer to the surface REF gives about 0.3 psu times higher salinity.

At Bornholm Deep (55.2 °N, 15.6 °E) in the next basin, the salinity from 40 m depth to the surface is almost constant and REF gives little more than 0.2 psu higher salinity

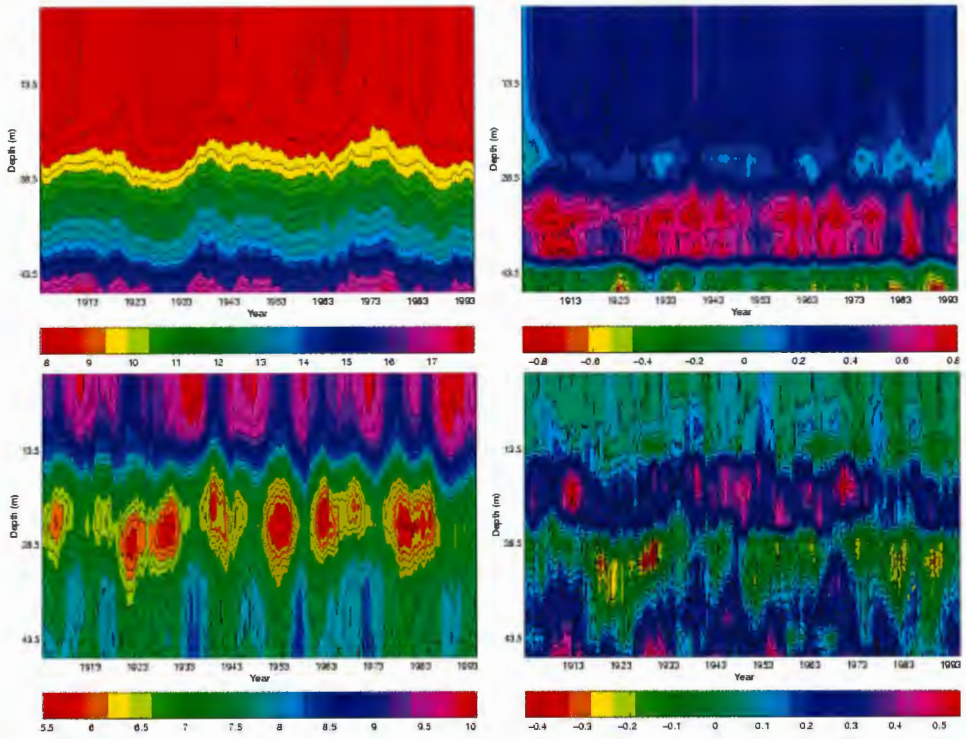

Figure 5.1: Arkona Deep, 47 m, 1905–1996. Upper left panel: The filtered reference salinity (in psu). Upper right panel: The filtered difference salinity, REF–FCT (in psu). Lower left panel: The filtered reference temperature (in °C). Lower right panel: The filtered difference temperature (in °C), REF–FCT. A 4-year running mean is used as a low-pass filter.

there (Fig.5.2). In the bottom layer FCT gives 0.2–1 psu higher salinity than REF. The fluctuations in the difference in the bottom layer seem not to be correlated with saltwater inflows from the North Sea.

At Gotland Deep it is visible that REF gives about 0.3 psu higher salinity than FCT above the halocline depth and FCT gives about 1 psu higher salinity than REF below the halocline depth, except for the spinup period (Fig.5.3). The spinup period is the time it takes before the effects of unrealistical initial fields have vanished. For salinity the spinup period is around 30 years. The halocline is the vertical layer with the largest vertical salinity gradient, located below the well-mixed homogeneous saline surface water layer. Note, that the plots at the Gotland Deep are not filtered because frequencies are smaller here than in the Arkona- and Bornholm Deep.

With plots from these three depths it is possible to see that the high saline water that comes from the North Sea diffuses vertically more for REF than for FCT. This is what can be expected because FCT's diffusion increases with the velocity, see section 3.4. To the contrary, REF has a constant explicit diffusion. When REF is compared to observations it has a tendency to overestimate the salinity above and underestimate it below the halocline. So it is good that FCT seems to have lower salinity above and higher salinity below the halocline.

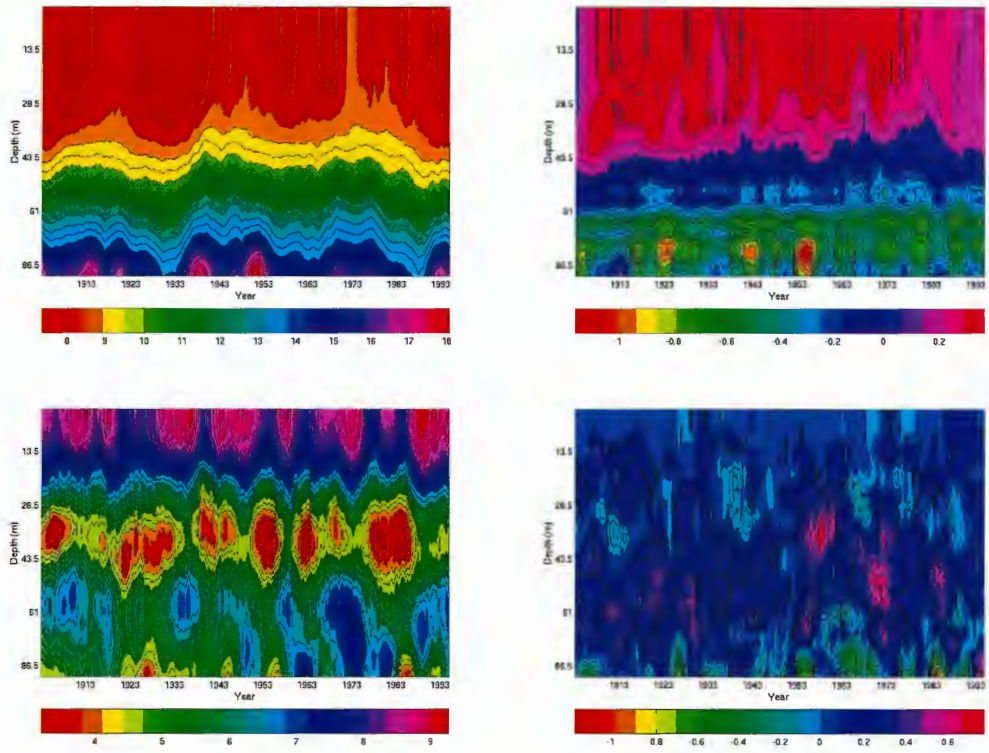

Figure 5.2: Bornholm Deep, 93 m, 1905–1996. Upper left panel: The filtered reference salinity (in psu). Upper right panel: The filtered difference salinity, REF–FCT (in psu). Lower left panel: The filtered reference temperature (in °C). Lower right panel: The filtered difference temperature REF–FCT (in°C). A 4-year running mean is used as a low-pass filter.

At Arkona Deep the temperatures are higher close to the bottom and a layer at 14–28 m, around 0.3 °C except for some years when the difference amounts to about 0.5 °C (Fig.5.1). Close to the surface there is almost no temperature difference between REF and FCT. At 28–40 m depth FCT gives 0.1–0.3 °C higher temperature, except for the years 1906–1915, 1935–1940, 1945–1948 and 1965–1970 when REF gives 0.2–0.3 °C higher temperature. These fluctuations in time do not seem to correlate with the stagnation periods. Stagnation periods are the time without major saltwater inflows from the North Sea. For information about major saltwater inflows see Meier and Kauker (2003).

At the Bornholm Deep the temperature is higher for REF, 0–0.3 °C, except for some shorter periods when FCT is higher close to the bottom, around 0.5 °C, and some short periods at 25–40 m, 0–0.3 °C (Fig.5.2). These periods seem not to be correlated with stagnation periods.

Figure 5.3 for the Gotland Deep contains more high frequency noise because it is not filtered. Above the halocline the difference is around 0 °C except for 1940–43 when FCT is 1–2 °C higher. Below the halocline FCT gives between 0–1 °C higher temperature, except for 1945–50 and 1965–70 when REF gives 0–0.5 °C higher temperature. There is

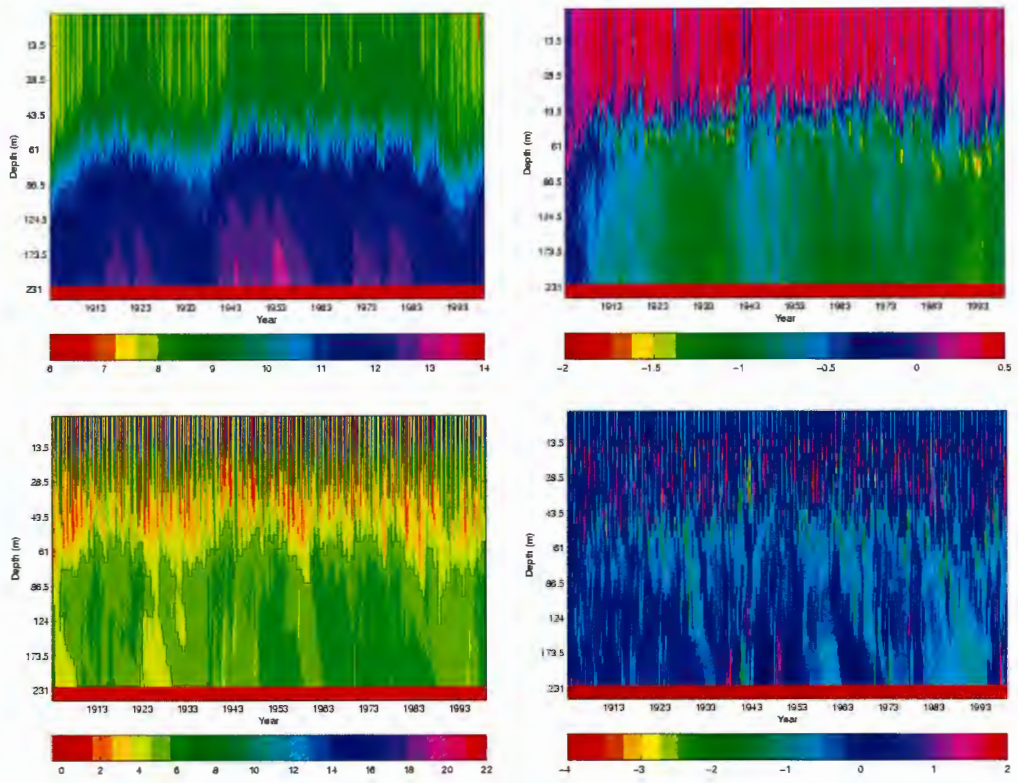

Figure 5.3: Gotland Deep, 231 m, 1903–1998. Upper left panel: The reference salinity (in psu). Upper right panel: The difference salinity, REF–FCT (in psu). Lower left panel: The reference temperature (in °C). Lower right panel: The difference temperature, REF–FCT (in °C).

no significant correlation between the difference plots and stagnation periods.

5.2 Salinity and temperature average as a function of time

A 3-dimensional average of salinity and temperature is calculated for the whole model domain every other day. The difference between the two models and a filtered difference is plotted in Figure 5.4. The same filter operator as above is used.

FCT gives greater average salinity and the difference increases with time, which was seen for the Gotland Deep. At the end of the simulated period FCT results in almost 0.2 psu higher average salinity. The inflow of saltwater through Kattegat is greater with FCT. The average of temperature is in the beginning 0.05 °C warmer with REF and oscillates around zero during the whole period.

The monthly average of salinity and temperature over the whole period is shown in Figure 5.5. The average is calculated for the whole model domain. FCT follows REF, but gives for the temperature somewhat lower, 0.1 °C, value for the coldest month March and somewhat warmer, 0.1 °C, for the warmest month August. FCT gives lower salinity during the year. The salinity difference has a very small annual variability, with a maximum

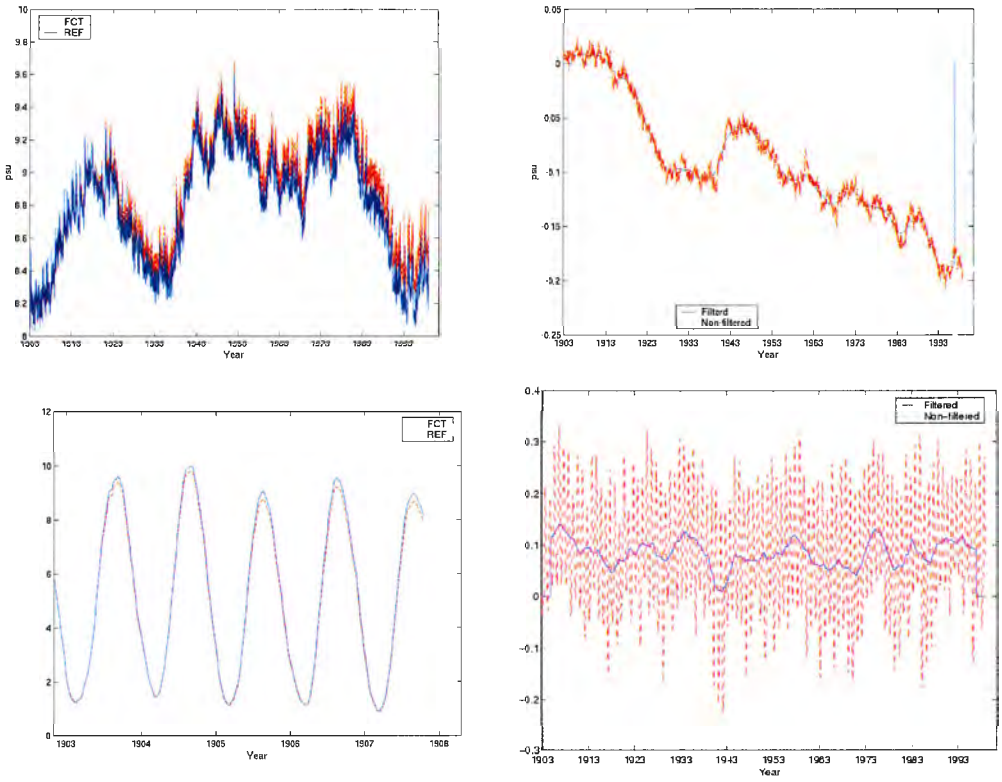

Figure 5.4: 1903–1998. Upper left panel: Spatial average salinity (in psu), REF (blue) and FCT (red). Upper right panel: Spatial average salinity difference (in psu), REF–FCT. The blue line is filtered with a four year running mean, the red line is non-filtered. Lower left panel: Spatial average temperature (in °C) for the first 10 years of the period, REF (blue) and FCT (red). Lower right panel: Spatial average temperature difference (in °C), REF–FCT. The blue line is filtered with a four year running mean and only calculated for 1905–1996. The red line is the non-filtered difference.

difference in September and October and a minimum difference in May.

5.3 Seasonal average for surface temperature and surface salinity

To see if there are any seasonal variations for the difference between REF and FCT the seasonal averages for winter and summer are calculated. For each year in the period 1903–1998 the time average is calculated for sea surface temperature (SST) and sea surface salinity (SSS). The average is calculated for winter (December–February) and summer (June–August). The time average is then calculated for the period 1903–1998. The results are shown in Figures 5.6 to 5.9

In winter the sea surface temperature is 0–0.1 °C warmer for FCT than REF along Sweden's east coast and along the coast inside the Gulf of Finland (Fig.5.6). In other parts

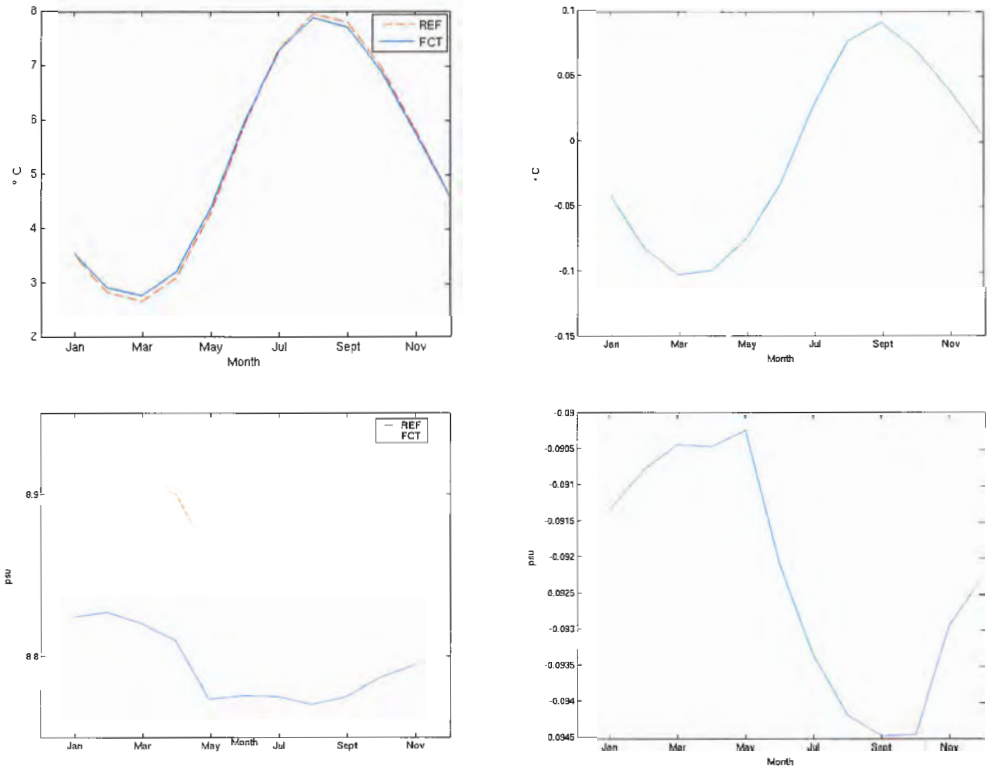

Figure 5.5: Monthly average, 1903–1998. Average for each month is calculated for the whole grid. Upper left panel: Temperature average (in °C). Upper right panel: Difference of temperature average, REF–FCT (in °C). Lower left panel: Salinity average (in psu), 1903–1998. Lower right panel: Difference of salinity average, REF–FCT (in psu).

REF gives 0–0.2 °C warmer sea surface temperature, except north east of Gotland, north of Poland and along the open boundary in Kattegat where the sea surface temperature is up to 0.5 °C warmer for REF.

In summer the average sea surface temperature differences are higher (Fig.5.7). FCT results in 0–0.5 °C higher sea surface temperatures in Kattegat. In the rest of the Baltic Sea REF gives higher sea surface temperatures. With 1–2 °C higher sea surface temperature in the Gulf of Bothnia, in the center of the Bothnian Sea and the eastern part of the Gulf of Finland. In other parts REF gives 0.2–1 °C higher sea surface temperatures. Differences of 1 °C and more are very big differences.

The sea surface salinity in winter calculated with FCT is about 0.5 psu higher in Little Belt, close to land along Sweden's west coast (Fig.5.8). In the Gulf of Bothnia and in the eastern part of the Gulf of Finland FCT gives 0–0.2 psu higher average sea surface salinity. REF gives higher sea surface salinity in and around the Gulf of Finland except for the far eastern part. In the rest of the Baltic Sea REF gives 0.3–0.5 psu higher average sea surface salinity.

In summer the sea surface salinity for FCT is higher (0–0.5 psu) only in Öresund, the eastern part of the Gulf of Bothnia and the most eastern part of the Gulf of Finland

(Fig.5.9). In Kattegat, Great- and Little Belt REF gives 1-2 psu higher sea surface salinity.

Figures 5.1 to 5.3 show that REF gives higher salinity above the halocline. Surface salinity gradients and surface salinity differences are largest in Kattegat, Öresund, Great- and Little Belt.

5.4 Average velocity field

Even though the advection of the velocity field is not changed in RCO velocities differ between FCT and REF. The reason is that salinity differs between the simulations and the amount of salinity effects density. Higher salinity causes higher density.

The time average sea surface velocity field for the whole period 1903–1998 is calculated. The reference velocity and the difference velocity are shown in Figure 5.10. The strongest signal from the difference plot is a stronger circulation around Gotland with FCT, by about 0.2 cm/s.

5.5 Surface salinity and surface temperature at the river mouths of Neva- and Kemijoki

One grid point is selected at the outflow of the Neva river in the Gulf of Finland and one from the Kemijoki river in the Gulf of Bothnia. In Figures 5.11 to 5.13 the sea surface temperature and the sea surface salinity are shown as a function of time for these points.

REF gives in the beginning negative values for sea surface salinity, both for Neva and Kemijoki rivers (Fig.5.11). This is unrealistic and comes from undershoots in REF at the large salt gradient when freshwater meets the saltwater. FCT handles, as expected, this large gradient without any undershoots. Similarly REF gives overshoots for the temperature in the summer time. Temperatures up to almost 35 °C in summer are not realistic close to the outflow of Neva in the Gulf of Finland (Fig.5.12). FCT has a maximum temperature of 25 °C in summer at the outflow of Neva.

At the outflow of Kemijoki river the temperature difference between the two methods is not that large as at the Neva river. Probably the gradient is larger at Neva and harder to handle for REF. Neva is the largest river into the Baltic Sea.

Sharp salinity and temperature gradients occur in the beginning of each simulation and are caused from the unrealistic initial fields. Even if the magnitude of the negative values for surface salinity is largest in the beginning of a simulation REF gives negative values during the whole period (Fig.5.11). There are also overshoots for the surface temperature for the whole period (Fig.5.12).

The reason that there are annual fluctuations in the salinity at the outflow of Kemijoki river but not at the outflow of Neva river might be that Neva's outflow ($2584 m^3/s$) is so strong that west winds cannot bring saltwater to its mouth. On the other hand Kemijoki's outflow ($593 m^3/s$) is not strong enough to prevent southern winds to bring some saltwater to its mouth.

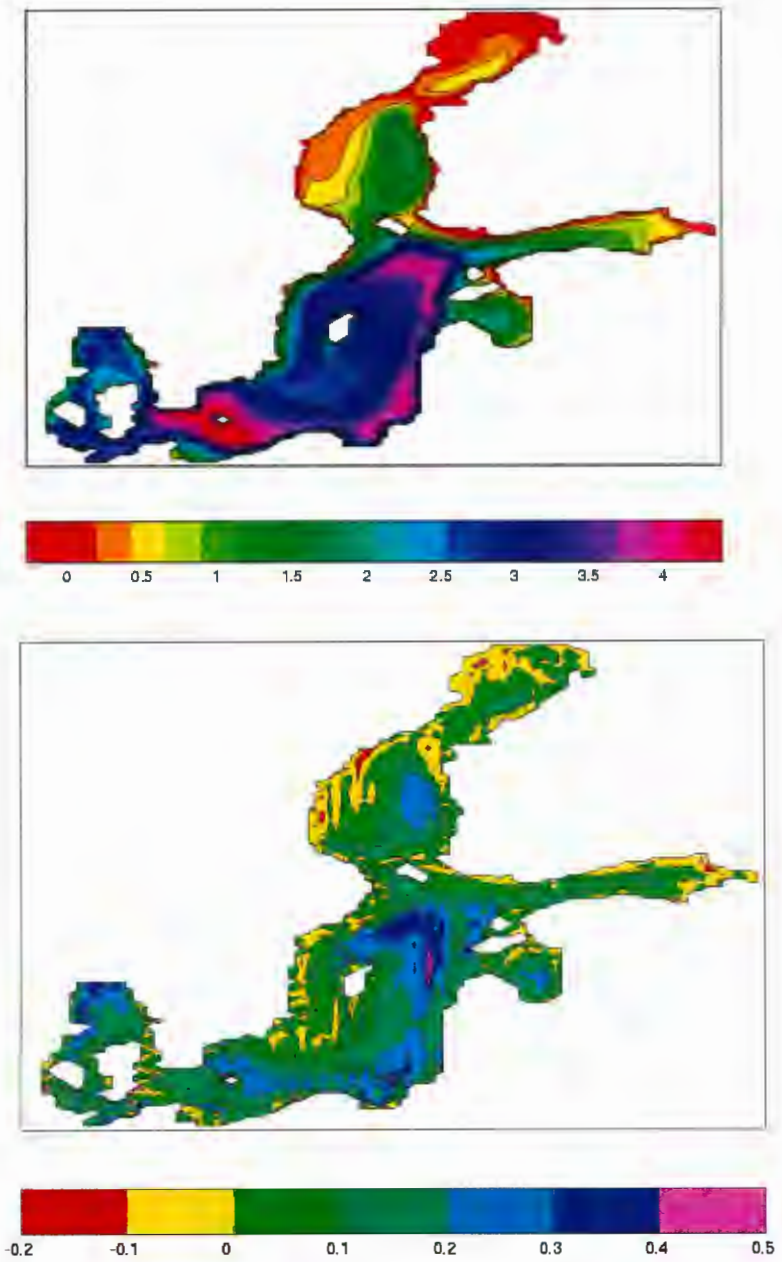

Figure 5.6: Seasonal average for sea surface temperature (in °C) in winter, for the period 1903-1998. Upper panel: REF. Lower panel: REF–FCT.

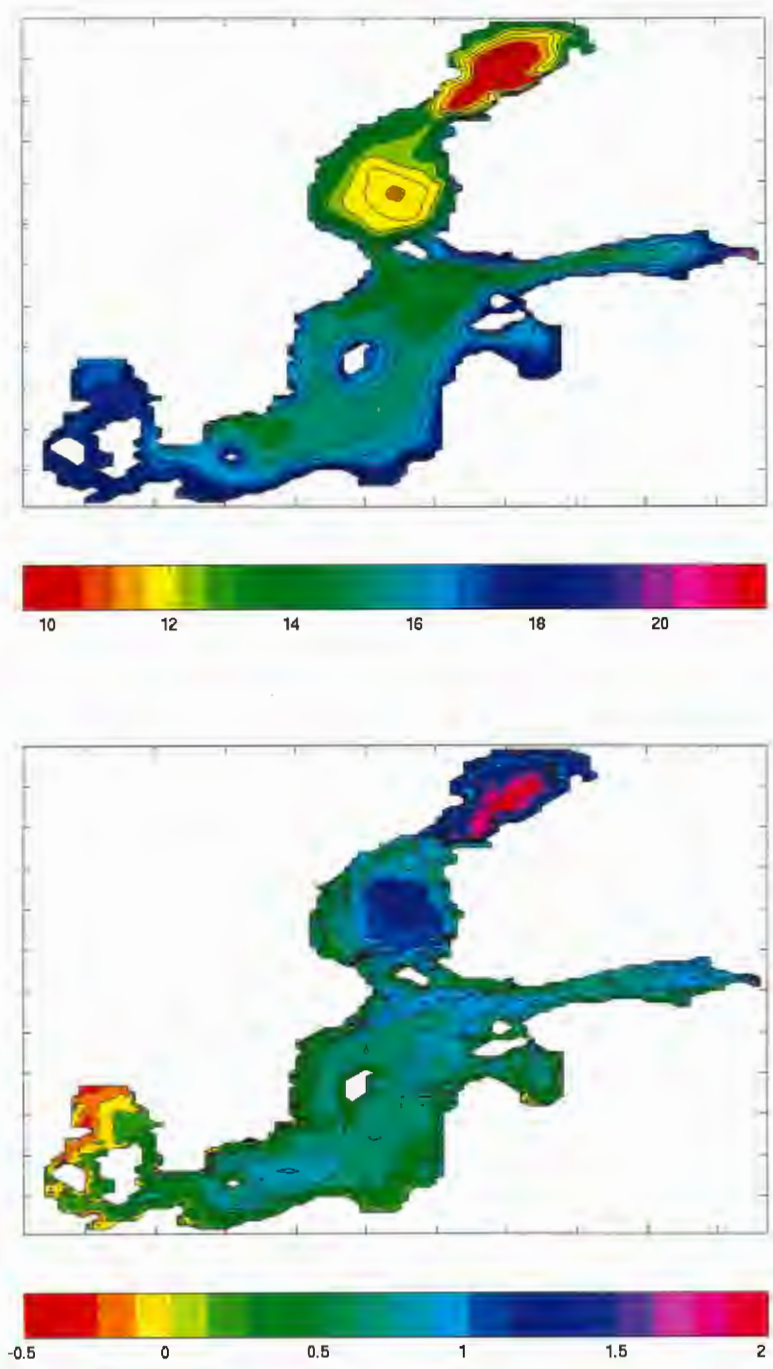

Figure 5.7: Seasonal average for sea surface temperature (in °C) in summer, for the period 1903-1998. Upper panel: REF. Lower panel: REF–FCT.

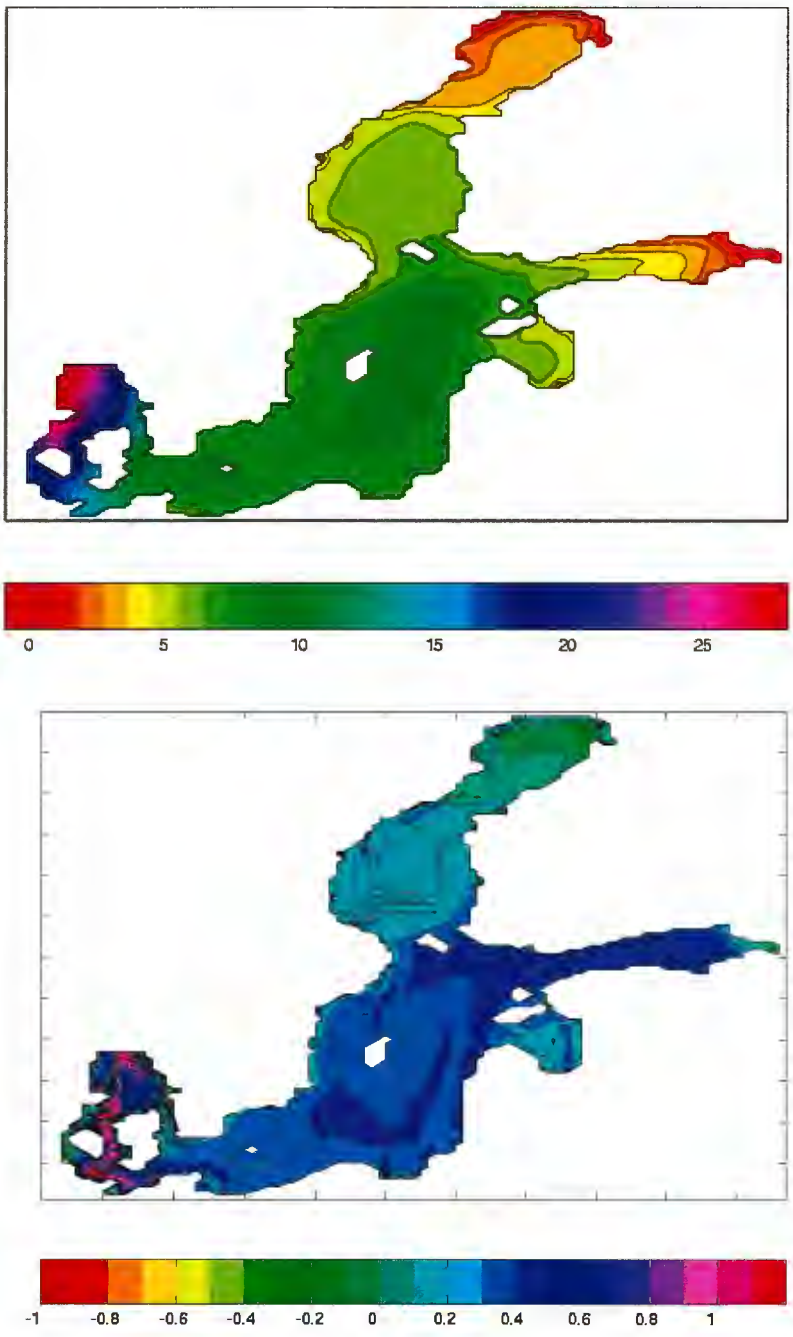

Figure 5.8: Seasonal average for sea surface salinity (in psu) in winter, for the period 1903-1998. Upper panel: REF. Lower panel: REF–FCT.

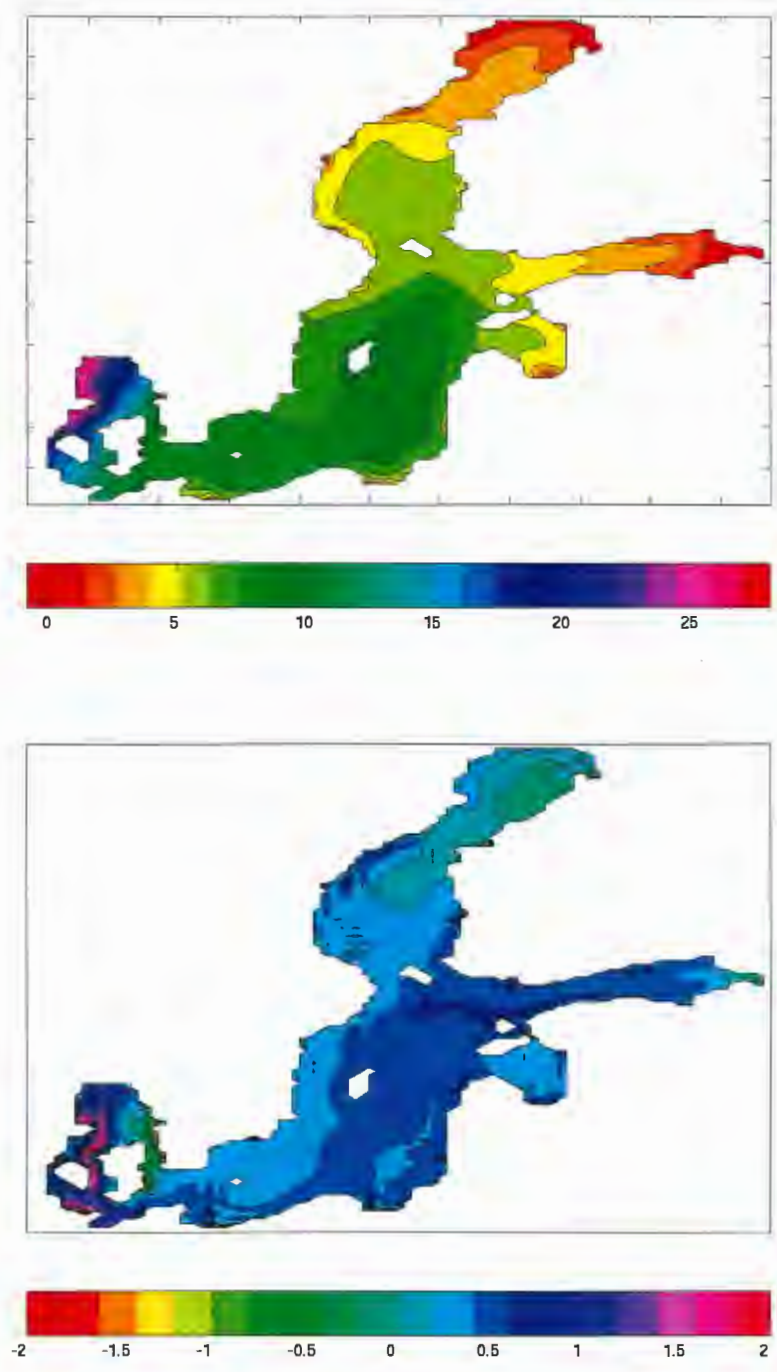

Figure 5.9: Seasonal average for sea surface salinity (in psu) in summer, for the period 1903-1998. Upper panel: REF. Lower panel: REF–FCT.

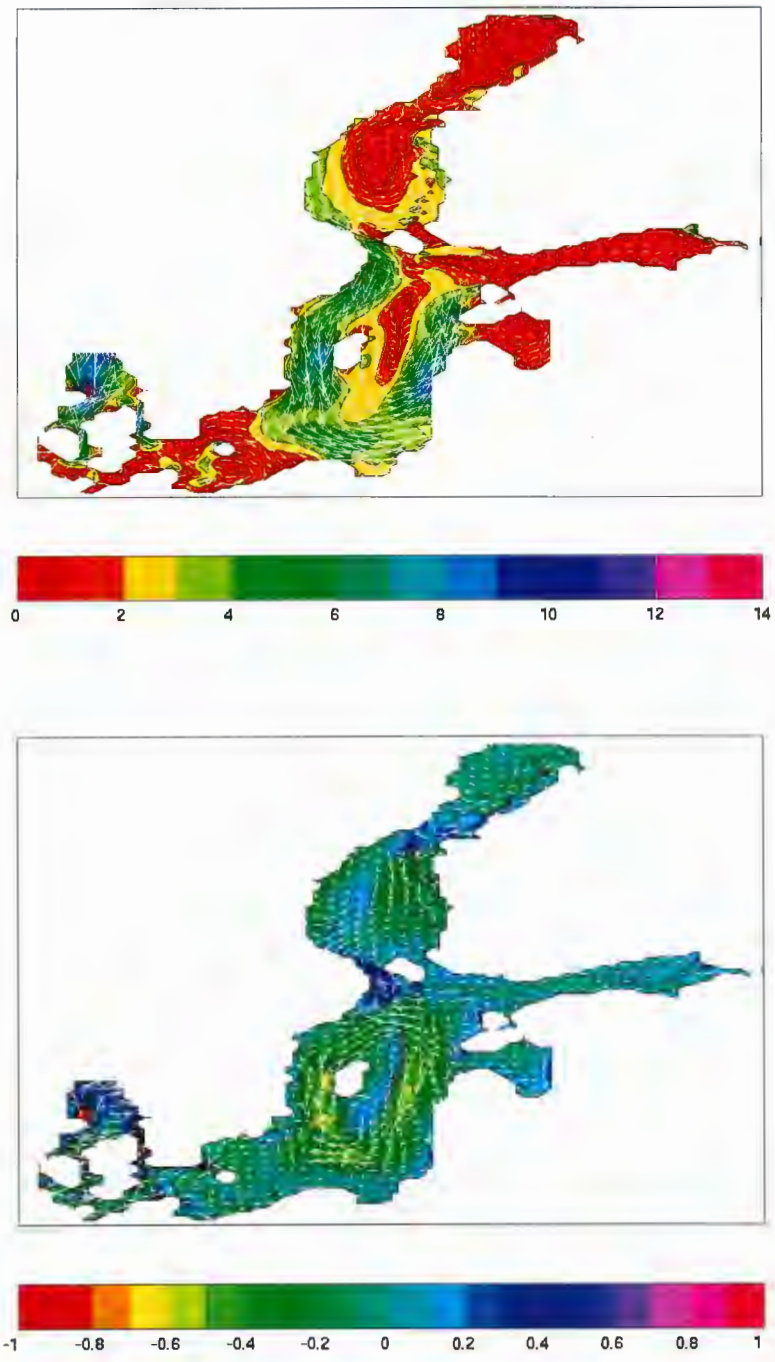

Figure 5.10: Average surface velocity field (in cm/s) for the period 1903–1998. The color bar shows the magnitude and the arrows shows the direction. Upper panel: REF. Lower panel: REF–FCT.

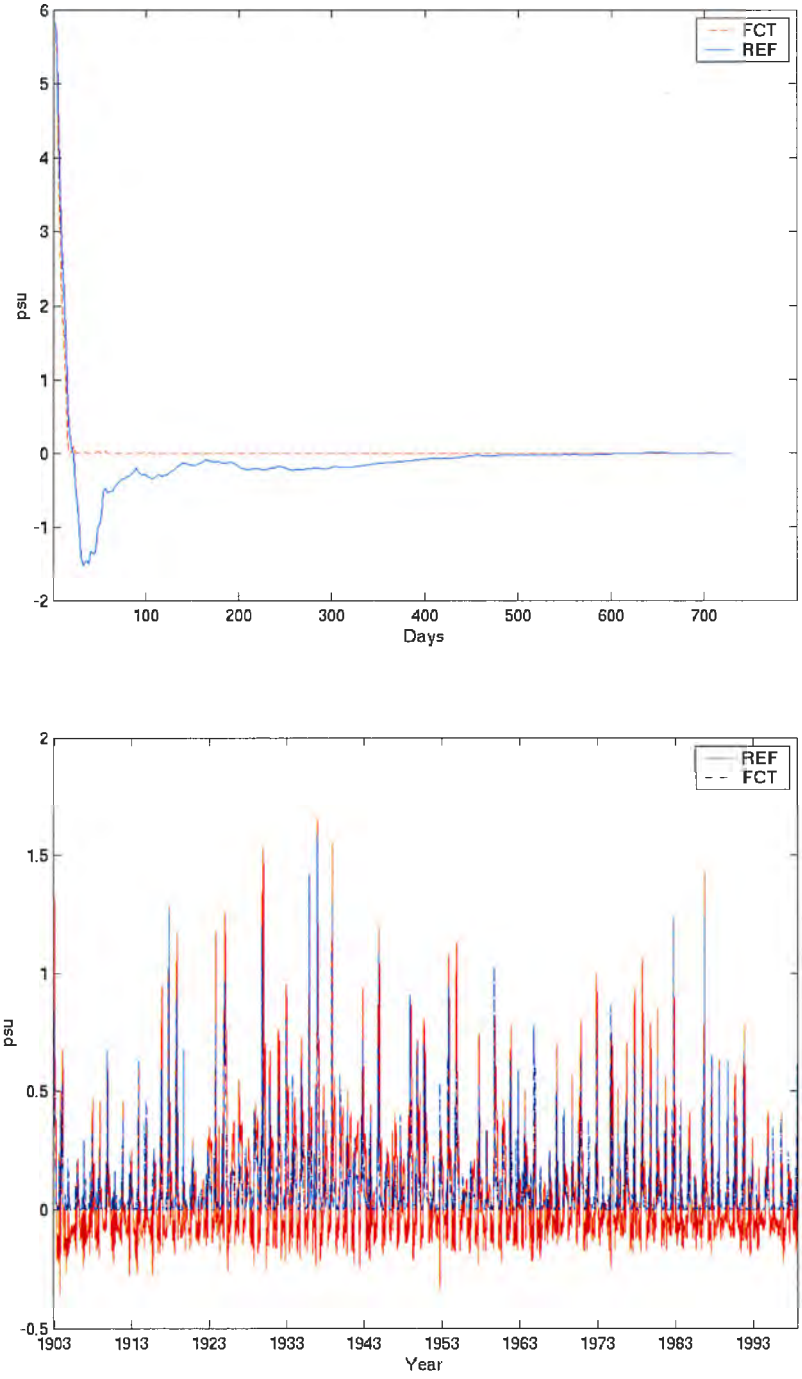

Figure 5.11: Sea surface salinity (in psu) at river outflows. Upper panel: Neva outflow for the first two years. Small negative values occur for REF during the whole period, 1903–1998. Lower panel: Kemijoki outflow for the whole period.

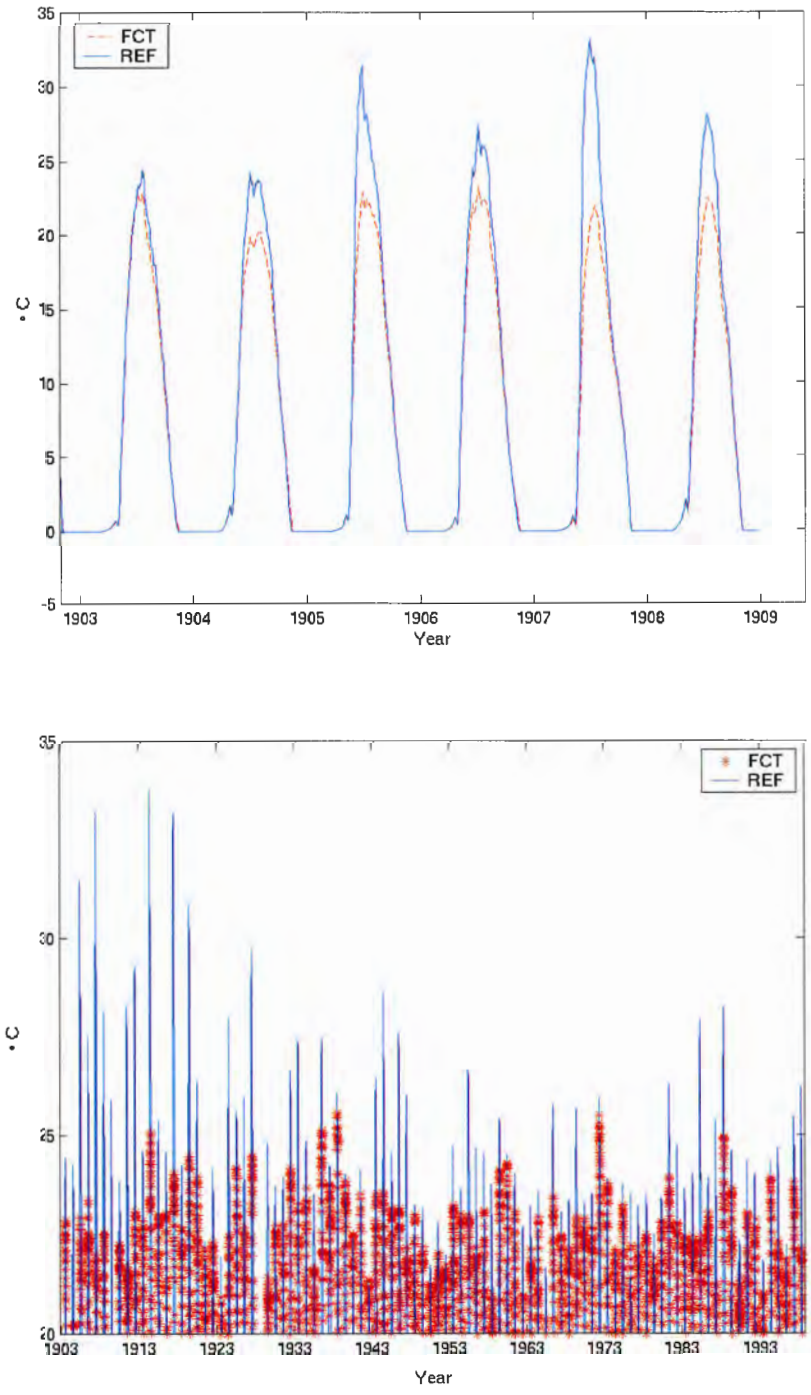

Figure 5.12: Sea surface temperature (in °C) at Neva river outflow for REF and FCT. Upper panel: For the period 1903–1909. Lower panel: For the period 1903–1998.

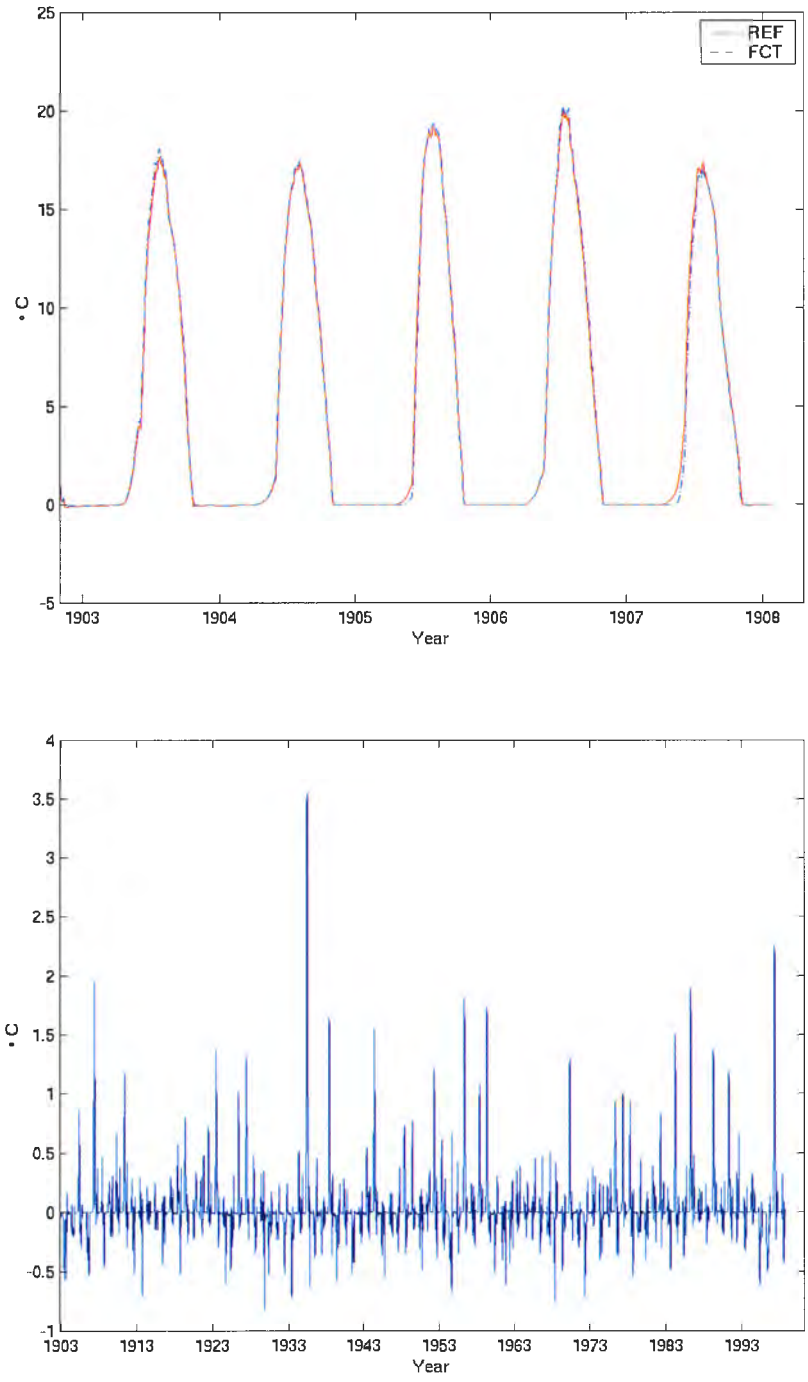

Figure 5.13: Sea surface temperature (in °C) at Kemijoki outflow. Upper panel: REF and FCT for the period 1903–1908. Lower: REF–FCT for the period 1903–1998.

Chapter 6

Conclusions

1. In section 3.1 the two advection schemes of FCT and incremental remapping were compared. It was found that incremental remapping preserved the shape of the density distribution better than FCT. Compared to central difference or upstream both FCT and incremental remapping give better results. It was found that incremental remapping is computationally more efficient than FCT only when more than 75 tracers are calculated. In RCO around 10 tracers are calculated. The computational cost and the fact that incremental remapping is not yet developed for three-dimensions means that FCT is the most realistic advection scheme to implement in RCO.

2. A stable FCT scheme has been implemented to RCO. One model simulation with 6nm(nautical miles) horizontal resolution from November 1902 to December 1998 was made. Preliminary analysis shows that RCO works satisfactory with the FCT scheme.

3. High salinity water that comes from the North Sea diffuses less vertically upward for FCT than for the RCO standard advection scheme that has been in use, modified split-quick. Modified split-quick must have a constant explicit diffusion to be stable. This leads to that the Arkona Deep, the Bornholm Deep and the Gotland Deep has higher salinity below the halocline for FCT. FCT has only implicit diffusion that increases with velocity and it gives low diffusion under the halocline. This is a positive effect, considering that as little diffusion as possible is desirable in the model.

4. At the outflows of the rivers Neva and Kemijoki the strong salinity gradient causes undershoots for REF, which creates negative salinity. Strong temperature gradients in the outflow of Neva causes overshoots for REF and unrealistic high temperatures. It was shown that FCT can handle the strong gradients at Neva and Kemijoki, and no negative salinity or unrealistic temperatures are calculated. That the salinity always is above zero is a desired feature in future applications as coupling RCO with a biogeochemical model.

Acknowledgment

First of all I would like to thank my supervisor Markus Meier at SMHI for giving me the chance to enter this interesting field. Thanks for your patience and guidance along the way.
I want to thank everyone at Rossby Centre at SMHI for always taking time. Especially I want to thank Ralf Döscher for valuable discussions.
Jonatan Strömgren thanks for comments on the report.
Many thanks to my wife Ida who have supported me a lot during my work.

Bibliography

CICE, 2003. Source-code. http://climate.lanl.gov/Models/CICE/index.htm.

Danielson, O., Haulin, J., 2004. Flux-corrected ocean tracer transport. Report in scientific computing advanced course, Dept. of Scientific Computing, Uppsala University.

Döös, K., 2004. Numerical methods in meteorology and oceanography. Tech. rep., Department of Meteorology, Stockholm University.

Dukowicz, J. K., Baumgardner, J. R., 2000. Incremental remapping as a transport/advection algorithm. Journal of Computational Physics 160, 318–335.

Dukowicz, J. K., Padial, N. T., 1991. Remap3d: A conservative three-dimensional remapping code. Tech. rep., Los Alamos National Laboratory, Los Alamos, New Mexico 87545.

Gerdes, R., 1988. Die Rolle der Dichtediffusion in numerischen Modellen der Nordatlantischen Zirkulation. Tech. Rep. 179, Berichte aus dem Institut für Meereskunde an der Christian-Albrechts-Universität, Kiel.

Gerdes, R., Köberle, C., Willebrand, J., 1991. The influence of numerical advection schemes on the results of ocean general circulation models. Climate Dynamics 5, 211–226.

Hunke, E. C., Lipscomb, W. H., 2004. CICE: the Los Alamos Sea Ice Model documentation and software user's manual. Tech. rep., T-3 Fluid Dynamics Group, Los Alamos National Laboratory, Los Alamos NM 87545.

Kunhardt, E. E., Wu, C., 1987. Towards a more accurate flux corrected transport algoritm. Journal of Computational Physics 68, 127–150.

Lipscomb, W. H., 2001. Remapping the thickness distribution in sea ice models. Journal of Geophysical Research 106, 989–1014.

Meier, H. E. M., Döscher, R., Coward, A., Nycander, J., Döös., K., 1999. RCO - Rossby Centre regional Ocean climate model model description. Tech. rep., SMHI, SE-601 76 Norrköping, Sweden.

Meier, H. E. M., Kauker, F., 2003. Modeling decadal variability of the baltic sea: 2. role of freshwater inflow and large-scale atmospheric circulation for salinity. J. Geophys. Res. 108, 3368.

Müller, P., Willebrand, J., 1989. Equations for oceanic motions. In: Sündermann, J. Landolt-Börnstein, Group V, Volume 3b. Springer Verlag.

Webb, D. J., Cuevas, B. A. D., Richmond, C. S., 1997. Improved advection schemes for ocean models. Journal of Atmospheric and Oceanic Technology 15, 1171–1187.

Zalesak, S. T., 1979. Fully multidimensional flux-corrected transport algorithms for fluids. Journal of Computational Physics 31, 335–362.

SMHIs publiceringar

SMHI ger ut sex rapportserier. Tre av dessa, R-serierna är avsedda för internationell publik och skrivs därför oftast på engelska. I de övriga serierna används det svenska språket.

Seriernas namn	**Publiceras sedan**
RMK (Rapport Meteorologi och Klimatologi)	1974
RH (Rapport Hydrologi)	1990
RO (Rapport Oceanografi)	1986
METEOROLOGI	1985
HYDROLOGI	1985
OCEANOGRAFI	1985

I serien OCEANOGRAFI har tidigare utgivits:

1 Lennart Funkquist (1985)
En hydrodynamisk modell för spridnings- och cirkulationsberäkningar i Östersjön Slutrapport.

2 Barry Broman och Carsten Pettersson. (1985)
Spridningsundersökningar i yttre fjärden Piteå.

3 Cecilia Ambjörn (1986).
Utbyggnad vid Malmö hamn; effekter för Lommabuktens vattenutbyte.

4 Jan Andersson och Robert Hillgren (1986).
SMHIs undersökningar i Öregrundsgrepen perioden 84/85.

5 Bo Juhlin (1986)
Oceanografiska observationer utmed svenska kusten med kustbevakningens fartyg 1985.

6 Barry Broman (1986)
Uppföljning av sjövärmepump i Lilla Värtan.

7 Bo Juhlin (1986)
15 års mätningar längs svenska kusten med kustbevakningen (1970 - 1985).

8 Jonny Svensson (1986)
Vågdata från svenska kustvatten 1985.

9 Barry Broman (1986)
Oceanografiska stationsnät - Svenskt Vattenarkiv.

11 Cecilia Ambjörn (1987)
Spridning av kylvatten från Öresundsverket

12 Bo Juhlin (1987)
Oceanografiska observationer utmed svenska kusten med kustbevakningens fartyg 1986.

13 Jan Andersson och Robert Hillgren (1987)
SMHIs undersökningar i Öregrundsgrepen 1986.

14 Jan-Erik Lundqvist (1987)
Impact of ice on Swedish offshore lighthouses. Ice drift conditions in the area at Sydostbrotten - ice season 1986/87.

15 SMHI/SNV (1987)
Fasta förbindelser över Öresund - utredning av effekter på vattenmiljön i Östersjön.

16 Cecilia Ambjörn och Kjell Wickström (1987)
Undersökning av vattenmiljön vid utfyllnaden av Kockums varvsbassäng.
Slutrapport för perioden
18 juni - 21 augusti 1987.

17 Erland Bergstrand (1987)
Östergötlands skärgård - Vattenmiljön.

18 Stig H. Fonselius (1987)
Kattegatt - havet i väster.

19 Erland Bergstrand (1987)
Recipientkontroll vid Breviksnäs fiskodling 1986.

20 Kjell Wickström (1987)
Bedömning av kylvattenrecipienten för ett kolkraftverk vid Oskarshamnsverket.

21 Cecilia Ambjörn (1987)
Förstudie av ett nordiskt modellsystem för kemikaliespridning i vatten.

22 Kjell Wickström (1988)
Vågdata från svenska kustvatten 1986.

23 Jonny Svensson, SMHI/National Swedish Environmental Protection Board (SNV) (1988)
A permanent traffic link across the Öresund channel - A study of the hydro-environmental effects in the Baltic Sea.

24 Jan Andersson och Robert Hillgren (1988)
SMHIs undersökningar utanför Forsmark 1987.

25 Carsten Peterson och Per-Olof Skoglund (1988)
Kylvattnet från Ringhals 1974-86.

26 Bo Juhlin (1988)
Oceanografiska observationer runt svenska kusten med kustbevakningens fartyg 1987.

27 Bo Juhlin och Stefan Tobiasson (1988)
Recipientkontroll vid Breviksnäs fiskodling 1987.

28 Cecilia Ambjörn (1989)
Spridning och sedimentation av tippat lermaterial utanför Helsingborgs hamnområde.

29 Robert Hillgren (1989)
SMHIs undersökningar utanför Forsmark 1988.

30 Bo Juhlin (1989)
Oceanografiska observationer runt svenska kusten med kustbevakningens fartyg 1988.

31 Erland Bergstrand och Stefan Tobiasson (1989)
Samordnade kustvattenkontrollen i Östergötland 1988.

32 Cecilia Ambjörn (1989)
Oceanografiska förhållanden i Brofjorden i samband med kylvattenutsläpp i Trommekilen.

33a Cecilia Ambjörn (1990)
Oceanografiska förhållanden utanför Vendelsöfjorden i samband med kylvatten-utsläpp.

33b Eleonor Marmefelt och Jonny Svensson (1990)
Numerical circulation models for the Skagerrak - Kattegat. Preparatory study.

34 Kjell Wickström (1990)
Oskarshamnsverket - kylvattenutsläpp i havet - slutrapport.

35 Bo Juhlin (1990)
Oceanografiska observationer runt svenska kusten med kustbevakningens fartyg 1989.

36 Bertil Håkansson och Mats Moberg (1990)
Glommaälvens spridningsområde i nordöstra Skagerrak

37 Robert Hillgren (1990)
SMHIs undersökningar utanför Forsmark 1989.

38 Stig Fonselius (1990)
Skagerrak - the gateway to the North Sea.

39 Stig Fonselius (1990)
Skagerrak - porten mot Nordsjön.

40 Cecilia Ambjörn och Kjell Wickström (1990)
Spridningsundersökningar i norra Kalmarsund för Mönsterås bruk.

41 Cecilia Ambjörn (1990)
Strömningsteknisk utredning avseende utbyggnad av gipsdeponi i Landskrona.

42 Cecilia Ambjörn, Torbjörn Grafström och Jan Andersson (1990)
Spridningsberäkningar - Klints Bank.

43 Kjell Wickström och Robert Hillgren (1990)
Spridningsberäkningar för EKA-NOBELs fabrik i Stockviksverken.

44 Jan Andersson (1990)
Brofjordens kraftstation - Kylvattenspridning i Hanneviken.

45 Gustaf Westring och Kjell Wickström (1990)
Spridningsberäkningar för Höganäs kommun.

46 Robert Hillgren och Jan Andersson (1991)
SMHIs undersökningar utanför Forsmark 1990.

47 Gustaf Westring (1991)
Brofjordens kraftstation - Kompletterande simulering och analys av kylvattenspridning i Trommekilen.

48 Gustaf Westring (1991)
Vågmätningar utanför Kristianopel - Slutrapport.

49 Bo Juhlin (1991)
Oceanografiska observationer runt svenska kusten med kustbevakningens fartyg 1990.

50A Robert Hillgren och Jan Andersson (1992)
SMHIs undersökningar utanför Forsmark 1991.

50B Thomas Thompson, Lars Ulander, Bertil Håkansson, Bertil Brusmark, Anders Carlström, Anders Gustavsson, Eva Cronström och Olov Fäst (1992).
BEERS -92. Final edition.

51 Bo Juhlin (1992)
Oceanografiska observationer runt svenska kusten med kustbevakningens fartyg 1991.

52 Jonny Svensson och Sture Lindahl (1992)
Numerical circulation model for the Skagerrak - Kattegat.

53 Cecilia Ambjörn (1992)
Isproppsförebyggande muddring och dess inverkan på strömmarna i Torneälven.

54 Bo Juhlin (1992)
20 års mätningar längs svenska kusten med kustbevakningens fartyg (1970 - 1990).

55 Jan Andersson, Robert Hillgren och Gustaf Westring (1992)
Förstudie av strömmar, tidvatten och vattenstånd mellan Cebu och Leyte, Filippinerna.

56 Gustaf Westring, Jan Andersson, Henrik Lindh och Robert Axelsson (1993)
Forsmark - en temperaturstudie. Slutrapport.

57 Robert Hillgren och Jan Andersson (1993)
SMHIs undersökningar utanför Forsmark 1992.

58 Bo Juhlin (1993)
Oceanografiska observationer runt svenska kusten med kustbevakningens fartyg 1992.

59 Gustaf Westring (1993)
Isförhållandena i svenska farvatten under normalperioden 1961-90.

60 Torbjörn Lindkvist (1994)
Havsområdesregister 1993.

61 Jan Andersson och Robert Hillgren (1994)
SMHIs undersökningar utanför Forsmark 1993.

62 Bo Juhlin (1994)
Oceanografiska observationer runt svenska kusten med kustbevakningens fartyg 1993.

63 Gustaf Westring (1995)
Isförhållanden utmed Sveriges kust - isstatistik från svenska farleder och farvatten under normalperioderna 1931-60 och 1961-90.

64 Jan Andersson och Robert Hillgren (1995)
SMHIs undersökningar utanför Forsmark 1994.

65 Bo Juhlin (1995)
Oceanografiska observationer runt svenska kusten med kustbevakningens fartyg 1994.

66 Jan Andersson och Robert Hillgren (1996)
SMHIs undersökningar utanför Forsmark 1995.

67 Lennart Funkquist och Patrik Ljungemyr (1997)
Validation of HIROMB during 1995-96.

68 Maja Brandt, Lars Edler och Lars Andersson (1998)
Översvämningar längs Oder och Wisla sommaren 1997 samt effekterna i Östersjön.

69 Jörgen Sahlberg SMHI och Håkan Olsson, Länsstyrelsen, Östergötland (2000).
Kustzonsmodell för norra Östergötlands skärgård.

70 Barry Broman (2001)
En vågatlas för svenska farvatten.

71 ***Vakant – kommer ej att utnyttjas!***

72 Fourth Workshop on Baltic Sea Ice Climate Norrköping, Sweden 22-24 May, 2002 Conference Proceedings
Editors: Anders Omstedt and Lars Axell

73 Torbjörn Lindkvist, Daniel Björkert, Jenny Andersson, Anders Gyllander (2003)
Djupdata för havsområden 2003

74 Håkan Olsson, SMHI (2003)
Erik Årnefelt, Länsstyrelsen Östergötland
Kustzonssystemet i regional miljöanalys

75 Jonny Svensson och Eleonor Marmefelt (2003)
Utvärdering av kustzonsmodellen för norra Östergötlands och norra Bohusläns skärgårdar

76 Eleonor Marmefelt, Håkan Olsson, Helma Lindow och Jonny Svensson, Thalassos Computations (2004)
Integrerat kustzonssystem för Bohusläns skärgård

77 Philip Axe, Martin Hansson och Bertil Håkansson (2004)
The national monitoring programme in the Kattegat and Skagerrak

78 Lars Andersson, Nils Kajrup och Björn Sjöberg (2004)
Dimensionering av det nationella marina pelagialprogrammet

79 Jörgen Sahlberg (2005)
Randdata från utsjön till kustzons-modellerna

80 Eleonor Marmefelt, Håkan Olsson (2005)
Integrerat Kustzonsystem för Hallandskusten

SMHI

Sveriges meteorologiska och hydrologiska institut
601 76 Norrköping
Tel 011 -495 80 00 · Fax 011-495 80 01

ISSN 0283-7714